

Research Article

Biosynthesis and characterization of a novel bismuth-based nanocatalyst for dye degradation: Experimental design, machine learning and ecotoxicity studies

Sth  fany Nunes Loureiro ^a, Daniel Moro Druzian ^a, Leandro Rodrigues Oviedo ^a, Cristiane dos Santos ^a, Yolice Patricia Moreno Ruiz ^b, Andr   Galembeck ^b, Giovani Pavoski ^c, Jorge Alberto Soares Ten  rio ^c, Denise Crocce Romano Espinosa ^c, William Leonardo da Silva ^{a,*}

^a Applied Nanomaterials Research Group (GPNAp), Franciscan University (UFN), Santa Maria, RS, Brazil

^b Department of Fundamental Chemistry (DQF), Federal University of Pernambuco (UFPE), Recife, PE, Brazil

^c Polytechnical School of Chemical Engineering, University of the São Paulo (USP), São Paulo, SP, Brazil

ARTICLE INFO

Keywords:

Dyes
Bismuth titanate
Nanoparticles
Heterogeneous photocatalysis
Green synthesis

ABSTRACT

The present study aims to synthesize and characterize a bismuth titanate nanostructure ($\text{Bi}_{12}\text{TiO}_{20}$ -NPs) from *Melissa officinalis* extract for degradation of fast green dye (FG). A machine learning (ML) study was performed to reduce the error associated with the central composite design rotational (CCDR 2³). Thus, the novelty of this work consists in correlating green nanotechnology (application of a green method for synthesizing a nanomaterial) with artificial intelligence (machine learning models) to predict the photocatalytic mechanism for the degradation of the fast green dye. The Artificial Neural Network (ANN) method was used, which indicates the prediction of percentage removal (R%) of the experimental data. $\text{Bi}_{12}\text{TiO}_{20}$ showed characteristic peaks of the perovskite and spherobismite phases, presence of functional groups of the Ti-O and Bi-O, V-type isotherm with H4 hysteresis, negative charge (-0.32 ± 0.02 mV), $\text{pH}_{ZCP} = 6.18$, band gap energy (Eg) of the 2.24 eV and morphology of rods and ellipses with an average particle size of 88.9 ± 24.8 nm. Doping with 2 wt% of magnesium chloride promoted an increase of about 37 % in photocatalytic activity ($k = 0.003\text{--}0.0086 \text{ min}^{-1}$), indicating a pseudo first-order kinetic model. Phytotoxicity tests were carried out to determine whether the samples would be toxic to *Lactuca sativa* and *Daucus carota* seeds, growth was observed in both solutions, doped and non-doped, indicating that the nanoparticle of $\text{Bi}_{12}\text{TiO}_{20}$ and $2\text{-MgBi}_{12}\text{TiO}_{20}$ is not toxic for the environment. Therefore, it was possible to produce an eco-friendly nanocatalyst by green synthesis for the photodegradation of food coloring.

1. Introduction

Water pollution and its unfavorable environmental and human health effects are of great concern [1]. In this way, Water pollution and its unfavorable effects on the environment as well as human health are of great concern [1]. Synthetic organic dyes are colored compounds that can chemically bond to the substrates to which they are used, where they have diverse applications in various industries such as textiles, cosmetics, cellulose and leather. [2]. Thus, the dyes (fast green – FG, methylene blue – MB and Rhodamine B – RhB) are chemically stable with high molecular weight, making removal difficult by conventional treatments requiring advanced treatments (e.g., adsorption, ozonation

and heterogeneous photocatalysis [3,4]). It is worth mentioning that the FG dye ($\text{C}_{37}\text{H}_{34}\text{N}_2\text{Na}_2\text{O}_{10}\text{S}_3$) is widely used in the printing, dyeing, cosmetics and medicine industries [5]. Moreover, its improper disposal of wastewater causes serious environmental problems due to its toxicity, carcinogenic and genotoxic [6].

Different techniques have been proposed and are being used to remove these toxic dyes from the aquatic system, such as adsorption, precipitation, electrocoagulation and chemical oxidation [7,8]. Among these methods, heterogeneous photocatalysis has been popularly adopted, as it is based on the principle of photoactivation of a semiconductor under ultraviolet and visible irradiation, providing the use of alternative materials [9]. Moreover, heterogeneous photocatalysis has received a

* Corresponding author.

E-mail address: williamleonardo_silva@hotmail.com (W.L. da Silva).

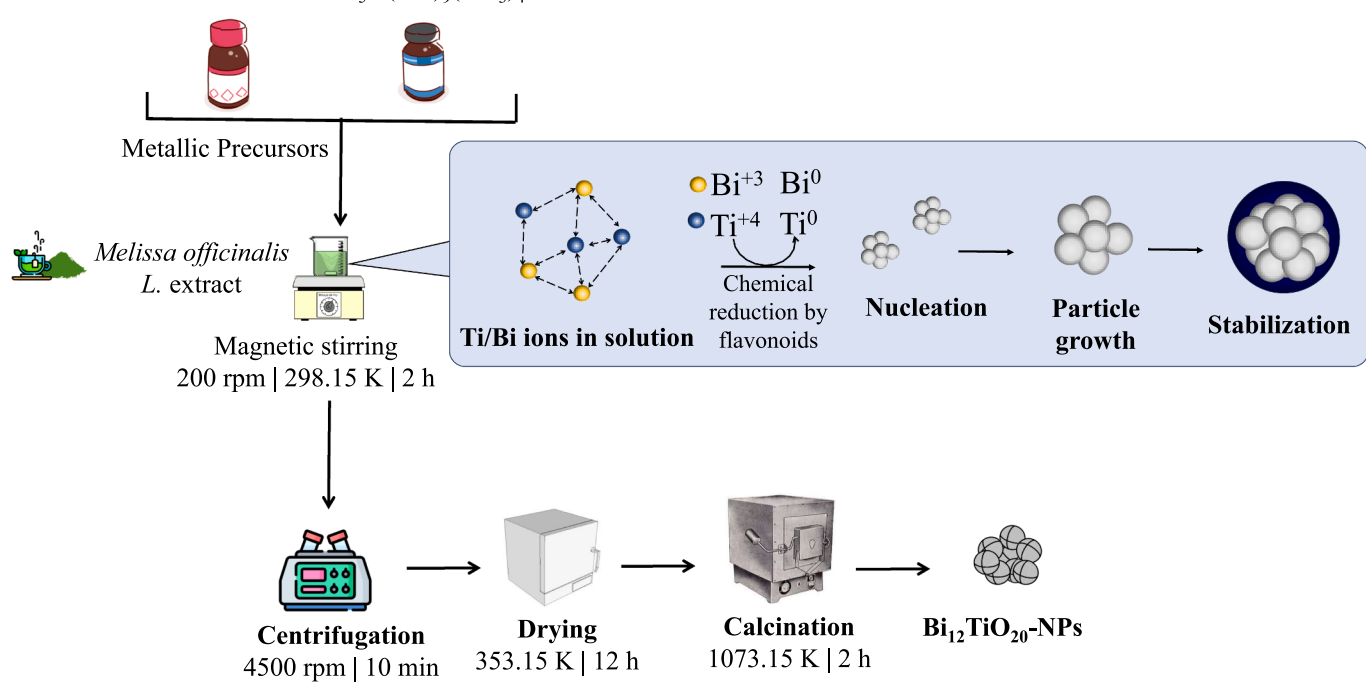


Fig. 1. Synthesis representation of $\text{Bi}_{12}\text{TiO}_{20}$ -NPs from *M. officinalis* extract using bismuth subnitrate and titanium (IV) isopropoxide.

lot of attention in recent years due to its promise to address pressing environmental issues and energy demands [10], such as photocatalytic water splitting (PWS) [11–13], solar water splitting [14], photocatalytic reduction reactions [15], carbonaceous materials in energy storage [16], highly active trifunctional electrocatalyst [17], Taguchi technique [18], photocatalytic hydrogen production [19] and photocatalytic H_2O_2 production [20].

Among the commercial catalysts used are titanium dioxide (TiO_2) and bismuth (III) oxide (Bi_2O_3) due to their favorable properties to act in the treatment of wastewater (mainly for fast green dye removal) [21,22]. Thus, bismuth titanate nanoparticles ($\text{Bi}_{12}\text{TiO}_{20}$) are denominated as a new class of promising candidates for wastewater treatment due to their excellent photocatalytic activity for the degradation of the organic pollutants and low band gap energy (around 2.3 eV) [23,24]. One of the main strategies to promote an increase in photocatalytic activity is doping with metallic ions to decrease the band gap energy, to promote better photoactivation and selectivity with the dye's molecules (i.e., electrostatic interactions) [25].

Green synthesis of Bi_2O_3 and TiO_2 has been used as an alternative method from plant extracts (e.g., *Mentha pulegium* and *Kniphofia foliosa*) which act as bioreducers of metallic precursors, followed by nucleation and stabilization of the nanoparticles [26,27]. It is noteworthy that the *Melissa officinalis* extract has strong antiviral, antibacterial, antidepressant and antispasmodic activities, associated with a high content of phenolic compounds (e.g., rosmarinic acid, quercetin, rutin, caffeic acid, chlorogenic acid and gallic acid), essential oils, vitamins and minerals [28,29].

Furthermore, the use of computational tools based on machine learning has been applied as an attractive alternative in elucidating the expected chemical reactions in wastewater treatment processes and in predicting the effectiveness of dye removal and nanocatalyst properties [30,31]. Thus, machine learning algorithms such as decision trees (DT), random forest (RF), K-Nearest Neighbors (KNN) and Multilayer Perceptron Artificial Neural Network (MLP-ANN) have shown promising results in the study of heterogeneous photocatalysis, reducing the costs associated with experimental procedures and time to carry out bench-scale studies [32,33].

In this context, this study aims to synthesize and characterize a bismuth titanate nanostructure ($\text{Bi}_{12}\text{TiO}_{20}$ -NPs) using *M. officinalis* extract for FG photodegradation under visible irradiation and to predict the degradation reaction pathway for the dye through the application of machine learning models. The novelty of this work is the use of a green process (biosynthesis) from a plant extract for the development of a new bismuth-based nanocatalyst, correlating the experimental tests of the experimental design with machine learning to determine the best operational condition by the heterogeneous photocatalysis process, reducing costs and time. In addition, it seeks to meet the sustainable development goals, specifically goal 6 (Ensure availability and sustainable management of water and sanitation for all), to improve water quality by treating wastewater containing dyes and minimizing the release of hazardous chemicals.

2. Materials and methods

2.1. Preparation of the *M. officinalis* extract

10 grams of *M. officinalis* leaves were collected from a local property (Santa Maria-RS, Brazil, $29^{\circ} 41' 29'' \text{ S}$, $53^{\circ} 48' 3'' \text{ W}$). The extract of *M. officinalis* was prepared using the infusion method [34]. The leaves were mixed with distilled water (100 mL) under magnetic stirring (300 rpm / $348.15 \pm 2 \text{ K}$) for 20 min

2.2. Biosynthesis of the bismuth titanate nanoparticles

Fig. 1 shows the $\text{Bi}_{12}\text{TiO}_{20}$ -NPs synthesis from *M. officinalis* extract by the biosynthesis method [35]. For the reduction and nucleation steps, 100 mL of the extract were added to 0.3 mol L^{-1} of titanium IV isopropoxide ($\text{Ti}[\text{OCH}(\text{CH}_3)_2]_4$, $\geq 97.0 \%$, Sigma-Aldrich®) and 0.3 mol L^{-1} of bismuth subnitrate ($\text{Bi}_5\text{O}(\text{OH})_9(\text{NO}_3)_4$, $\geq 98.0 \%$, Sigma-Aldrich®) under magnetic stirring (200 rpm for 120 min). Then, for the stabilization step, centrifugation was used (4500 rpm for 10 min), followed by drying ($353.15 \pm 2 \text{ K}$ for 720 min) and calcination ($1073.15 \pm 2 \text{ K}$ for 120 min / 5 K min^{-1}).

Table 1Independent variables with maximum and minimum limits used by CCRD 2³.

Order	FG (mg L ⁻¹)	Bi ₁₂ TiO ₂₀ -NPs (g L ⁻¹)	pH
(-1.68)	15.9	0.13	2
(-1)	50	0.30	4
0	100	0.55	7
(+1)	150	0.8	10
(+1.68)	184.1	0.97	12

2.3. *M. officinalis* extract characterization

To characterize *M. officinalis* extract, high-performance liquid chromatography (HPLC) was used to determine its composition, where LabSolutions data processing system was used with a C18 reverse column (3.9 × 150 mm, and 4 µL). Thus, gradient elusion consisted of two mobile phases (i) water (99.7 %) and formic acid (0.3 %); and (ii) methanol (99.7 %) and formic acid (0.03 %). The detection wavelength was 280 nm, and the flow rate was 1.0 mL min⁻¹. Moreover, each injection volume was 20 µL and the column temperature was maintained at ambient conditions (298.15 ± 2 K). The retention time (RT), and C (concentration) were available.

2.4. Bi₁₂TiO₂₀-NPs characterizations

To identify the crystalline phases, a diffractometer Bruker (model D2 Advance) with a copper tube ($\lambda_{\text{Cu}-\alpha} = 0.15418$ nm) was used ranging from 5° to 70° with an acceleration voltage of 30 kV and applied current of 30 mA. Crystalline structure was analyzed using the JCPDS database (Joint Committee on Powder Diffraction Standards) and calculated the average crystallite size (d_c – Eq. (1)) and interplanar distance (d – Eq. (2)) [36,37].

$$d_c = \frac{0.94 * \lambda_{\text{Cu}-\alpha}}{\beta * \cos(\theta)} \quad (1)$$

$$d = \frac{\lambda_{\text{Cu}-\alpha}}{2 * \text{sen}(\theta)} \quad (2)$$

Where: β is the total width at half maximum (FWHM); and θ is the Bragg diffraction angle (°).

The identification of the functional groups was obtained by Fourier transform infrared spectra (FTIR) in a Perkin Elmer Spectrum Frontier in transmittance mode of 4000 and 500 cm⁻¹ with 45 scans and 2 cm⁻¹ resolution. Morphological properties were determined by Field Emission Gun – Scanning Electron Microscope (FEG-SEM) in a Microscope MIRA3 (TESCAN) and the particle size distribution was calculated using the software ImageJ®. Elemental analysis was determined using a Scanning Electron Microscope with Energy Dispersive X-ray Spectrometer (brand X PHENO, model PROX 2020) operating at 15 kV. N₂ porosimetry was used to determine the textural properties (e.g., surface area, pore diameter and pore volume) with relative pressure in the range of P/P₀¹ = 0 to 1 measured by the Brunauer-Emmett-Teller (BET) and Barrett-Joyner-Halenda (BJH) methods [38] in a Micromeritics ASAP 2020 Plus instrument. Zeta potential (ZP) was determined using the

Table 3Main metabolite compounds identified by HPLC of the *M. officinalis* extract.

Component	RT (min)	Area (%)	Concentration (µg mL ⁻¹)
Rosmarinic acid	1.614	37.54	7.50
catechin	1.853	25.03	5.00
luteolin	2.426	16.96	3.39
caffeoic acid	3.199	6.16	1.23
ferulic acid	3.560	4.13	0.83
gallic acid	4.609	3.79	0.76
chlorogenic acid	4.725	2.94	0.59
gallic acid	5.524	0.91	0.18
syringic acid	6.950	0.13	0.03
citronellol	8.084	0.17	0.04
hesperidin	8.675	2.24	0.45

RT is the retention time, and C is the concentration.

Table 2

Technical details of machine learning algorithms.

Algorithm	Algorithm parameters	Equations	Reference
Decision Tree (DT)	Tree maximum depth: 5, 10, 20, 30; minimum number of splits per tree: 2, 5, 10, 15; minimum samples leaf: 1, 2, 4, 6; and performance measured by minimizing the mean squared error R(T), according to Eq. (11)	$R(T) = \frac{1}{N} \sum_{t \in T} \sum_{i \in t} (y_i - \hat{y}_i)^2$ (11) Where: R(T) is the expected value of the sum of mean squared errors using a constant as a predictive model; N is the number of nodes used in the decision/pattern recognition in the data (one node is equivalent to one leaf of the decision tree); y _i is the observed value obtained experimentally; \hat{y}_i is the predicted value obtained from the model; t is the identifier of each node; and T is the mean squared error between the observed and the predicted values (response)	[48]
Random Forest (RF)	Number of decision trees tested: 50, 100, 200; tree maximum depth: 5, 10, 20, 30; minimum number of splits per tree: 2, 5, 10, 15; minimum samples leaf: 1, 2, 4, 6; and performance measured by minimizing the mean squared error R ₁ (T), as defined in DT algorithm	$R_1(T) = \frac{1}{N} \sum_{t \in T} \sum_{i \in t} (y_{1i} - \hat{y}_{1i})^2$ (12) Eq. (12) but using more than one decision tree, with n-repartitions of the trees, density in a group of k-elements, generating a particular answer (decision i, j, k). The algorithms use optimization functions that guarantee greater computational power, fast convergence to the optimal value predicted by the algorithm and less probability of overfitting; Response is the average of the decisions of the n-groups made up of k-trees	[49]
K-Nearest Neighbors (KNN)	Weight: uniform, distance; algorithm: KD tree, ball tree; K-neighbors: 1, 2, 3; exponent associated with metric distance: p = 0.5, 0.8, 1; and performance measured by minimizing the Euclidean distance, according to Eq. (13)	$D(X, Y) = \sqrt{\sum_{i=1}^N (y_i - \hat{y}_i)^2}$ (13) Where: D(X, Y) is the Euclidean distance (for each test point, the algorithm finds the k nearest neighbors in the training set using a distance measure and predicts the value for the test point as the average of the values of the k nearest neighbors); N is the data size; y _i is the observed value obtained experimentally; and \hat{y}_i is the predicted value obtained from the model	[50]
Multilayer Perceptron Artificial Neural Network (MLP-ANN)	Neural network structure: m:n:k, where m is the number of input data (independent variables); n is the number of neurons in the hidden layer, Main node function: summation/activation function used in each node (Eq. 14), associated with ReLu (Eq. 15), logistic (Eq. 16), and hyperbolic (Eq. 17) functions; Weight optimization: Adam**, SGD***, and RMSProp****	$\varphi = \sum w_n \bullet x_n + b_k$ (14) $f(\varphi) = (0, x_{max})$ (15) $f(\varphi) = \frac{1}{1 - e^{-\varphi}}$ (16) $f(\varphi) = \frac{2}{1 + e^{-2\varphi}} - 1$ (17) Where: φ is the transfer function; x _n is the neural network node; w _n is the weight associated with the neuron x _n ; b _k is the bias (error associated with the prediction model); x _{max} is the maximum value predicted by the ANN algorithm, using the ReLu function	[51]

cv = 5 for all algorithms tested | * Parameter associated with the learning rate of the algorithm | ** Adaptive Moment Estimation function | *** Stochastic Gradient Descent function and **** Root Mean Squared Propagation

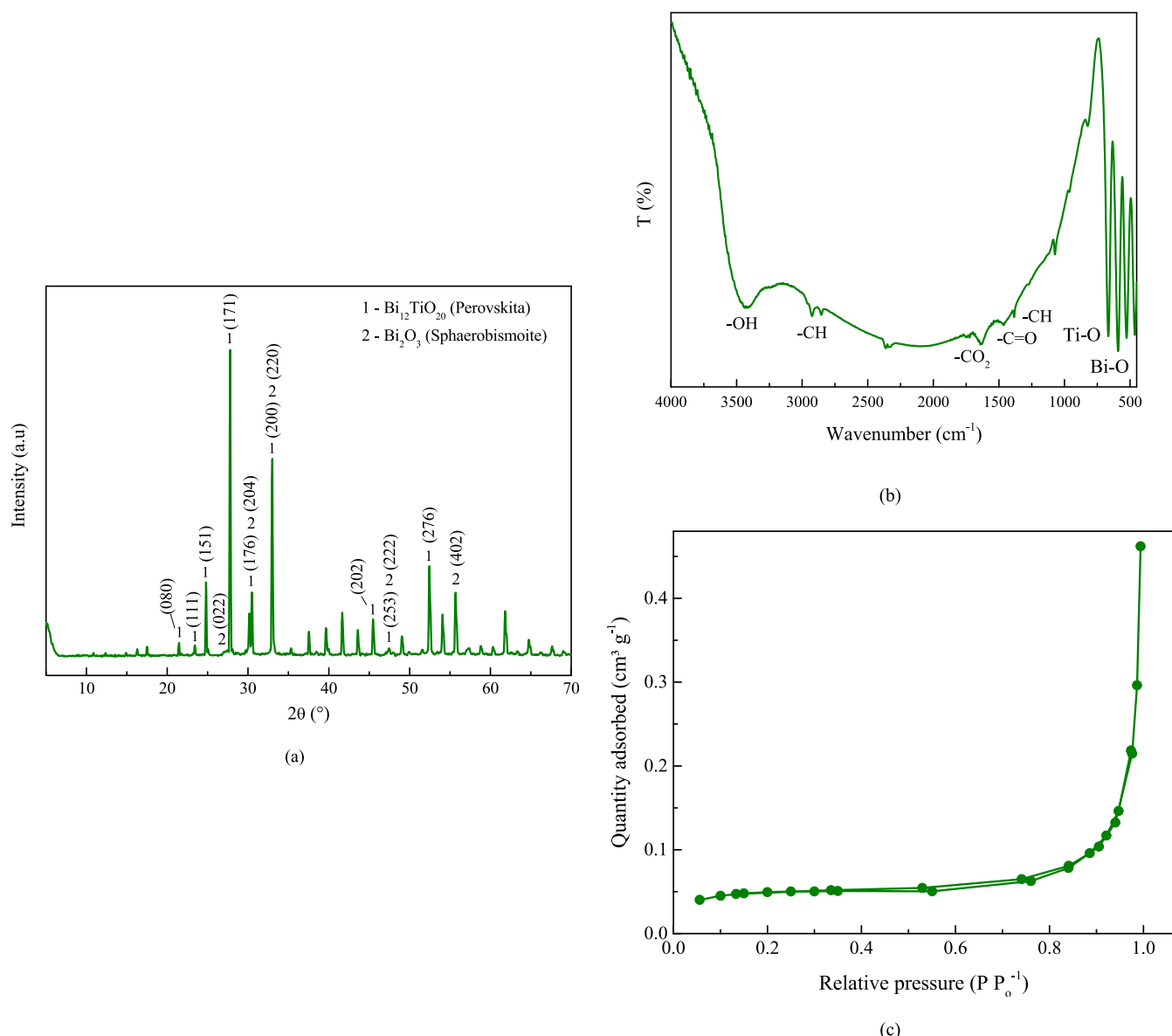


Fig. 2. (a) XRD diffractogram and (b) FTIR spectra of the $\text{Bi}_{12}\text{TiO}_{20}$ -NPs (c) N_2 adsorption/desorption isotherms of the $\text{Bi}_{12}\text{TiO}_{20}$ -NPs, (d) zero charge point of the $\text{Bi}_{12}\text{TiO}_{20}$ -NPs and (e) Tauc plot generated from Kubelka-Munk equation of the $\text{Bi}_{12}\text{TiO}_{20}$ -NPs.

nanoZS Malvern-Zetasizer® model (ZEN3600, UK). For the pH_{ZCP} tests, the method of 11 tests was used [39]. Thermal properties were investigated by Thermogravimetric analysis (TGA) curves and Derived Thermogravimetry (DTG) in a thermogravimetric analyzer (Shimadzu, model TGA-60/60H) using a platinum sample port and synthetic air with a gas flow of 100 mL min^{-1} , in a temperature range of $298.15\text{--}1273.15 \text{ K}$ with a heating rate of 10 K min^{-1} . UV-vis spectrum was carried out in a Varian Cary 100 Scan Spectrophotometer (with an accessory DRA-CA-301-Labsphere) in the diffuse reflectance mode to determine the band gap energy by the Kubelka–Munk function Tauc plot $-(F(R)h\nu)^n$ versus $h\nu$, with $n = 0.5$ or 2 , Eqs. (3)–(5) ranging from 200 to 800 nm [40].

$$F(R) = \frac{(1 - R_{\infty})^2}{2R_{\infty}} \quad (3)$$

$$h\nu = \frac{1240}{\lambda} \quad (4)$$

$$R = \frac{1}{A} \quad (5)$$

Where: $F(R)$ is the Kubelka–Munk function; R_{∞} is the reflectance (a.u.); $h\nu$ is the incident photon energy (eV); λ is the wavelength associated with the maximum absorbance (nm) of the sample. The exponent n is considered 0.5 for direct and 2 for indirect transitions.

2.5. Experimental design by CCRD

To determine the ideal condition of the heterogeneous photocatalysis process for the FG photodegradation, CCRD 2^3 was carried out, where the independent variables were the dye concentration, catalyst concentration and the reaction pH, while the response variable was dye removal percentage (%R), according to the Table 1.

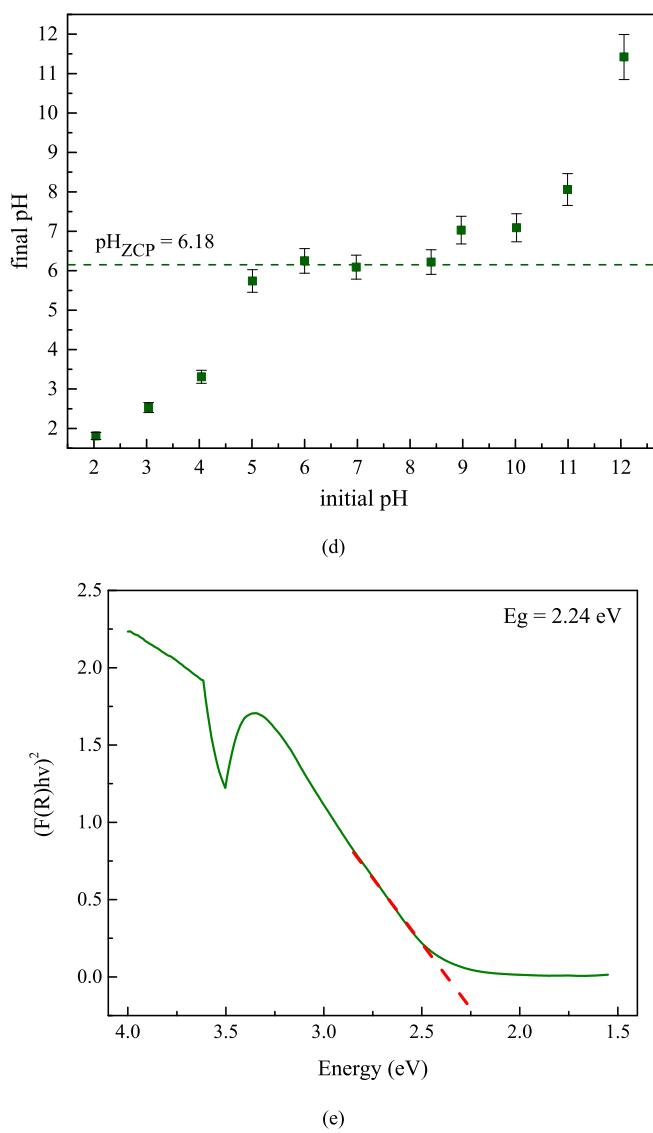


Fig. 2. (continued).

2.6. Photocatalytic tests

FG dye was used as a pollutant target and Bi₁₂TiO₂₀-NPs as a catalyst for photocatalytic tests. The tests were carried out in two steps: (i) 60 min in the dark phase (without irradiation); and (ii) photocatalysis step under visible irradiation, where aliquots were collected at 0–180 min, filtered ($\phi = 0.45 \mu\text{m}$) and diluted (1:10 v v⁻¹). UV-vis spectroscopy was used to evaluate the FG photodegradation in a Spectrophotometer Shimadzu 1280 at $\lambda = 622 \text{ nm}$ [41].

2.7. Photodegradation kinetics

The kinetic study of the FG photodegradation was carried out under visible light irradiation using the Langmuir-Hinshelwood model [42,43] to determine the apparent rate of the pseudo first-order reaction (k), according to the Eqs. (6) and (7):

$$(-r_i) = -\frac{dC_i}{dt} = \frac{k_s^* K^* C_i}{1 + K^* C_i} \quad (6)$$

$$C_i = C_{i0}^* e^{-k^* t} \quad (7)$$

Where: K (L mol⁻¹) is the adsorption constant; k_s (mol L⁻¹ min⁻¹) is the

apparent constant of reaction; C_{i0} (mol L⁻¹) is the initial FG dye concentration; C_i (mol L⁻¹) is the FG concentration; k (min⁻¹) is the apparent rate of the pseudo first-order reaction; and t (min) is the reaction time.

2.8. Effect of doping of Bi₁₂TiO₂₀-NPs

The doping effect was used for possible improvements in photocatalytic activity of Bi₁₂TiO₂₀-NPs, where the impregnation method was used [44,45]. Thus, 100 mL of distilled water was added with MgCl₂ and Bi₁₂TiO₂₀ (1–25 wt%) under stirring magnetic (250 rpm / 90 min). After, the sample was dried (353.15 K / 12 h) and calcined (773.15 K / 2 h / 5 K min⁻¹). It is noteworthy that doping was used to aim for higher efficiency in the photodegradation of the FG dye due to the smaller atomic radius of magnesium ions, allowing an increase in interactions with FG [46].

2.9. Phytotoxicity tests

The phytotoxicity assay was carried out using *Lactuca sativa* and *Daucus carota* seeds [47]. Thus, in a petri dish with germinating paper (Germitest®), several solutions (0.1, 0.01, 0.0010, 0.0050 mg L⁻¹) of the

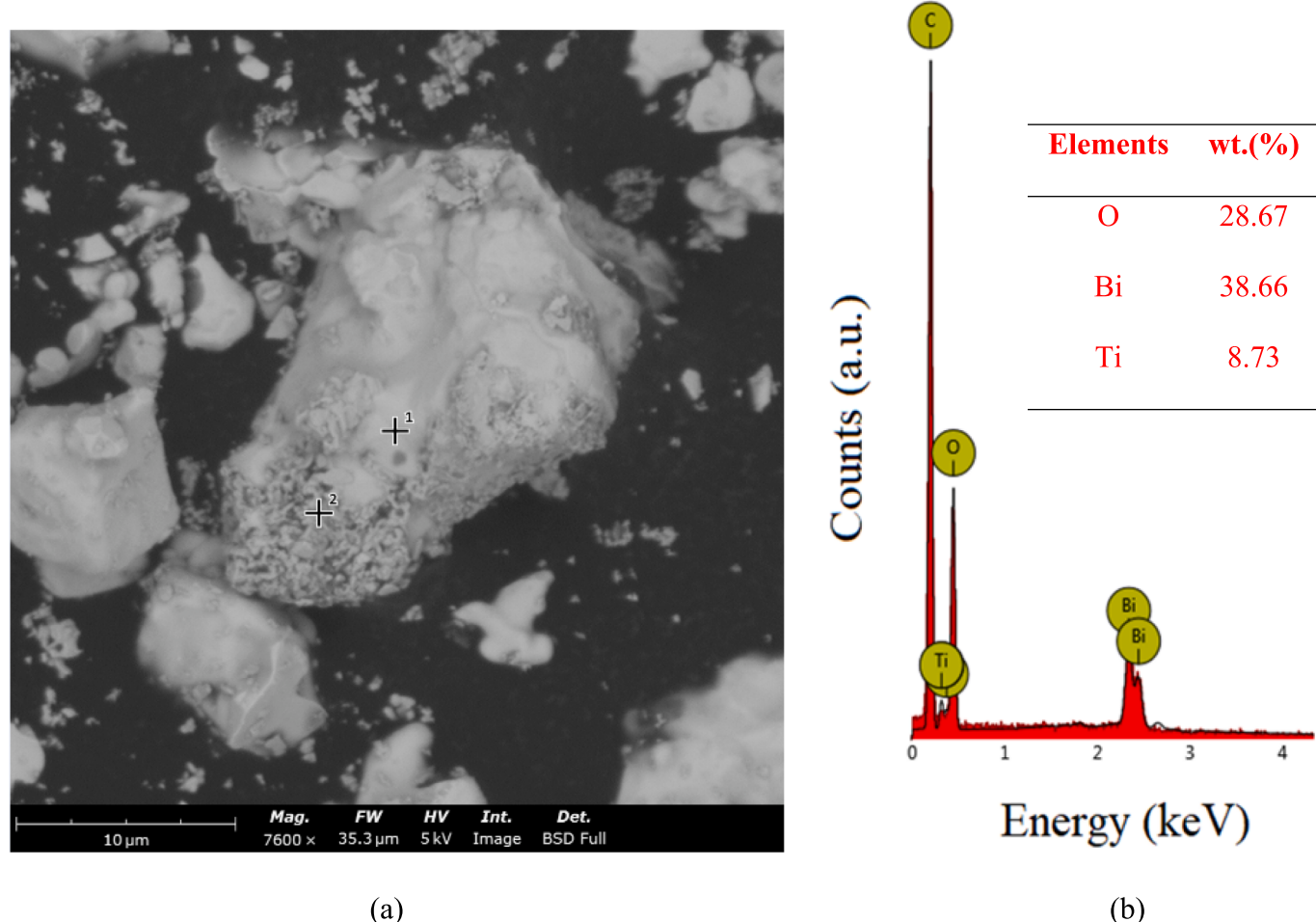


Fig. 3. (a) SEM micrography of $\text{Bi}_{12}\text{TiO}_{20}$ -NPs with 7600x magnification, (b) EDX results, (c and d) FEG-SEM micrographs of $\text{Bi}_{12}\text{TiO}_{20}$ -NPs with 5kx and 25kx magnification, respectively; and (e) average particle size of $\text{Bi}_{12}\text{TiO}_{20}$ -NPs.

$\text{Bi}_{12}\text{TiO}_{20}$ -NPs and $\text{MgCl}_2\text{-Bi}_{12}\text{TiO}_{20}$ -NPs were placed with seeds for 168 h with controlled humidity. Measurements were realized with a digital caliper (Mitsuyo®).

2.10. Statistical analysis

Results of independent experiments are expressed as arithmetic mean \pm standard deviation (SD). Data were analyzed using one-way analysis of variance (ANOVA) followed by Tukey's multiple comparison tests. Differences between groups were rated significantly at * $p < 0.05$, ** $p < 0.01$, *** $p < 0.001$ and **** $p < 0.0001$. All analyses were carried out using the GraphPad Prism7.0® software.

2.11. Machine learning

A supervised machine learning (ML) study was carried out to predict the dye removal for values beyond the experimental runs to achieve higher degradation values and to address the influence of the photo-catalytic parameters on FG removal. Thus, six algorithms were used to achieve these goals: K-Nearest Neighbors (KNN), Support Vector Machine (SVM), Decision Tree (DT), Random Forest (RF), and Multilayer Perceptron Artificial Neural Network (MLP-ANN). The algorithms were coded and compiled in Python 3.8 (Google Colaboratory open-source version), using 6 input variables (reaction time, pH, [Catalyst], [Dye], doping agent, and doping percentage) and 1 output variable (%R). The library scikit-learn was for the compilation of the vector and tree-based

machine learning models and metrics evaluation, whereas tensorflow and keras were used to construct and run the artificial neural network, respectively. The dataset (file Loureiro_et_al_2024.xlsx, with 442 rows and 7 columns) was provided on GitHub (https://github.com/Lean_droOviedo/Machine-and-Deep-Learning), where 20 % of the dataset was used for testing. The training and testing data were further normalized with the importation and use of the preprocessing and Standard Scaler functions from the scikit-learn library, using the command MaxMinScaler to normalize data in the range between 0 and 1. Table 2 shows the configurations of each ML algorithm used in this work.

The metrics adopted to validate the performance of the ANN were the coefficient of determination (R^2), the root means squared error (RMSE), and the average relative error (ARE) as presented in Eq. (8), Eq. (9), and Eq. (10) respectively.

$$R^2 = 1 - \frac{\sum_{i=1}^N (y_{i,\text{exp}} - y_{i,\text{pred}})^2}{\sum_{i=1}^N (y_{i,\text{exp}} - \hat{y}_{i,\text{pred}})^2} \quad (8)$$

$$\text{RMSE} = \sqrt{\frac{\sum_{i=1}^N (y_{i,\text{exp}} - \hat{y}_{i,\text{pred}})^2}{N}} \quad (9)$$

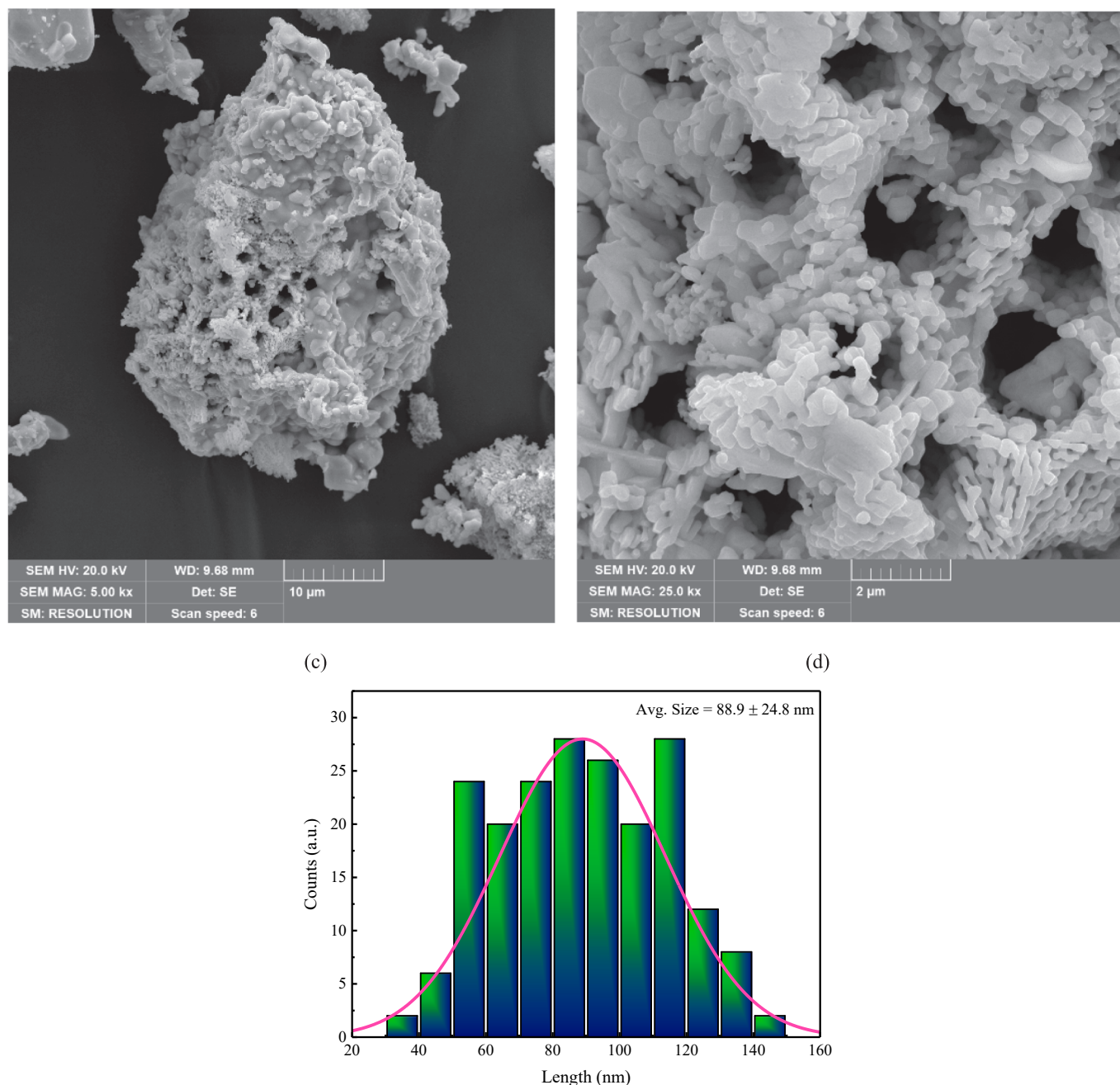


Fig. 3. (continued).

$$ARE = 100 \left| \frac{(y_{i,\text{exp}} - \hat{y}_{i,\text{pred}})}{y_{i,\text{exp}}} \right| \quad (10)$$

Where: $y_{i,\text{exp}}$, $\hat{y}_{i,\text{pred}}$ and $\hat{y}_{i,\text{pred}}$ are the observed value, the predicted value, and the average of the predicted value of the output variable (Removal – %R); N is the data size used in the machine learning study.

3. Results and discussion

3.1. Characterization of the *M. officinalis* extract

Table 3 shows the HPLC results from *M. officinalis* extract, where it was possible to identify the presence of rosmarinic acid (RT = 1.614 min and C = 7.50 μg mL⁻¹), catechin (RT = 1.853 min and C = 5 μg mL⁻¹), luteolin (RT = 2.426 min and C = 3.39 μg mL⁻¹), caffeic acid (RT =

3.199 min and C = 1.23 μg mL⁻¹), ferulic acid (RT = 3.560 min and C = 0.83 μg mL⁻¹), gallic acid (RT = 4.609 min and C = 0.76 μg mL⁻¹), chlorogenic acid (RT = 4.725 min and C = 0.59 μg mL⁻¹), gallic acid (RT = 5.524 min and C = 0.18 μg mL⁻¹), syringic acid (RT = 6.950 min and C = 0.03 μg mL⁻¹), citronellol (RT = 8.084 min and C = 0.04 μg mL⁻¹) and hesperidin (RT = 8.675 min and C = 0.45 μg mL⁻¹) [52,53]. It is noteworthy that the *M. officinalis* extract has a high antioxidant activity indicating that components, for example flavonoids (catechin, luteolin, citronellol and hesperidin) have the potential for application as a bioreductive agent in biosynthesis for the formation of nanoparticles.

3.2. Characterization of the Bi₁₂TiO₂₀-NPs

Fig. 2(a)–(e) present the X-ray diffractogram, FTIR spectrum, N₂ adsorption/desorption isotherms, zero charge point, DRS spectrum and

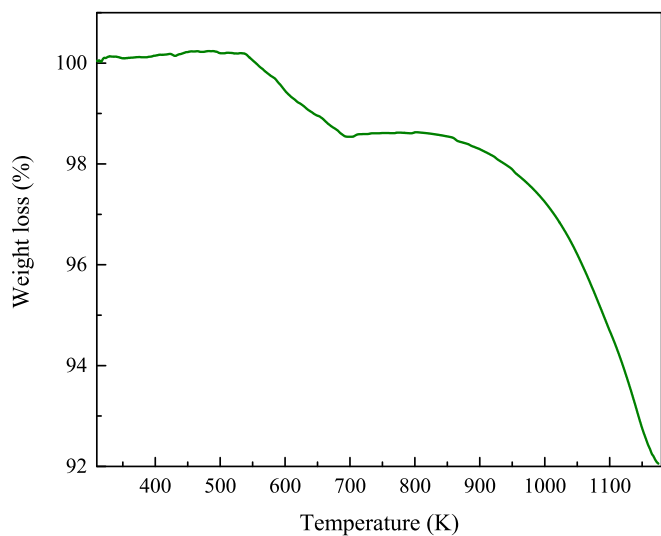


Fig. 4. TGA thermogram of the $\text{Bi}_{12}\text{TiO}_{20}$ -NPs.

Table 4
CCDR 2^3 for FG photodegradation by heterogeneous photocatalysis using $\text{Bi}_{12}\text{TiO}_{20}$ -NPs.

[FG] (mg L^{-1})	[$\text{Bi}_{12}\text{TiO}_{20}$ -NPs] (g L^{-1})	pH	%R
40	0.06	7	6.04
20	1.0	4	14.41
40	0.65	7	15.73
40	1.24	7	19.87
40	0.65	12	20.83
6.36	0.65	7	19.06
40	0.65	2	9.00
40	0.65	7	6.87
73.63	0.65	7	23.83
20	0.3	4	13.54
20	1.0	10	9.17
60	0.3	10	9.96
60	1.0	4	37.36
60	0.3	4	9.78
60	1.0	10	24.58
20	0.3	10	26.37
40	0.65	7	8.33

Tauc plot generated from Kubelka-Munk equation of the $\text{Bi}_{12}\text{TiO}_{20}$ -NPs, respectively.

Fig. 2(a) shows the crystalline phases, where $\text{Bi}_{12}\text{TiO}_{20}$ -NPs showed peaks of the perovskite phase ($\text{Bi}_4\text{Ti}_3\text{O}_{12}$, JCPDS n° 34-0097) with 2θ at 22.94° (080, $d = 4.10 \text{ \AA}$), 23.25° (111, $d = 3.90 \text{ \AA}$), 25.92° (151, $d = 3.60 \text{ \AA}$), 28.81 (171, $d = 3.30 \text{ \AA}$), 30.09° (176, $d = 3.10 \text{ \AA}$), 32.85° (200, $d = 2.80 \text{ \AA}$), 46.64° (202, $d = 2.01 \text{ \AA}$), 47.02° (253, $d = 2.00 \text{ \AA}$) and 52.95° (276, $d = 1.79 \text{ \AA}$); and sphaerobismite phase (Bi_2O_3 , JCPDS n° 27-0050) with crystalline peaks at 27.94° (022, $d = 3.30 \text{ \AA}$), 31.72° (204, $d = 2.90 \text{ \AA}$), 32.70° (220, $d = 2.84 \text{ \AA}$), 46.20° (222, $d = 2.04 \text{ \AA}$) and 57.74° (402, $d = 1.66 \text{ \AA}$). $\text{Bi}_{12}\text{TiO}_{20}$ -NPs demonstrated an average crystallite size in both phases around 27–30 nm, similar to that found in the literature, suggesting a nanometric scale and confirming the biosynthesis of bismuth titanate [54].

Fig. 2(b) showed the FTIR spectra, where the $\text{Bi}_{12}\text{TiO}_{20}$ -NPs presented chemical groups of hydroxyl functional groups (O-H) at 3310 cm^{-1} ; -C-H vibration of the aldehyde group at 2825 cm^{-1} ; intermolecular hydrogen water at 1630 cm^{-1} ; -CO₂ due to air atmospheric at 1628 cm^{-1} ; C=O and C-H stretching of the carboxylic acid group at 1425 cm^{-1} and 1342 cm^{-1} denoted in extract *M. officinalis*, respectively; and vibrational stretching of the Ti-O and Bi-O types at 822 cm^{-1} and 588 cm^{-1} , respectively [55].

Fig. 2(c) shows the N_2 adsorption/desorption isotherms, where

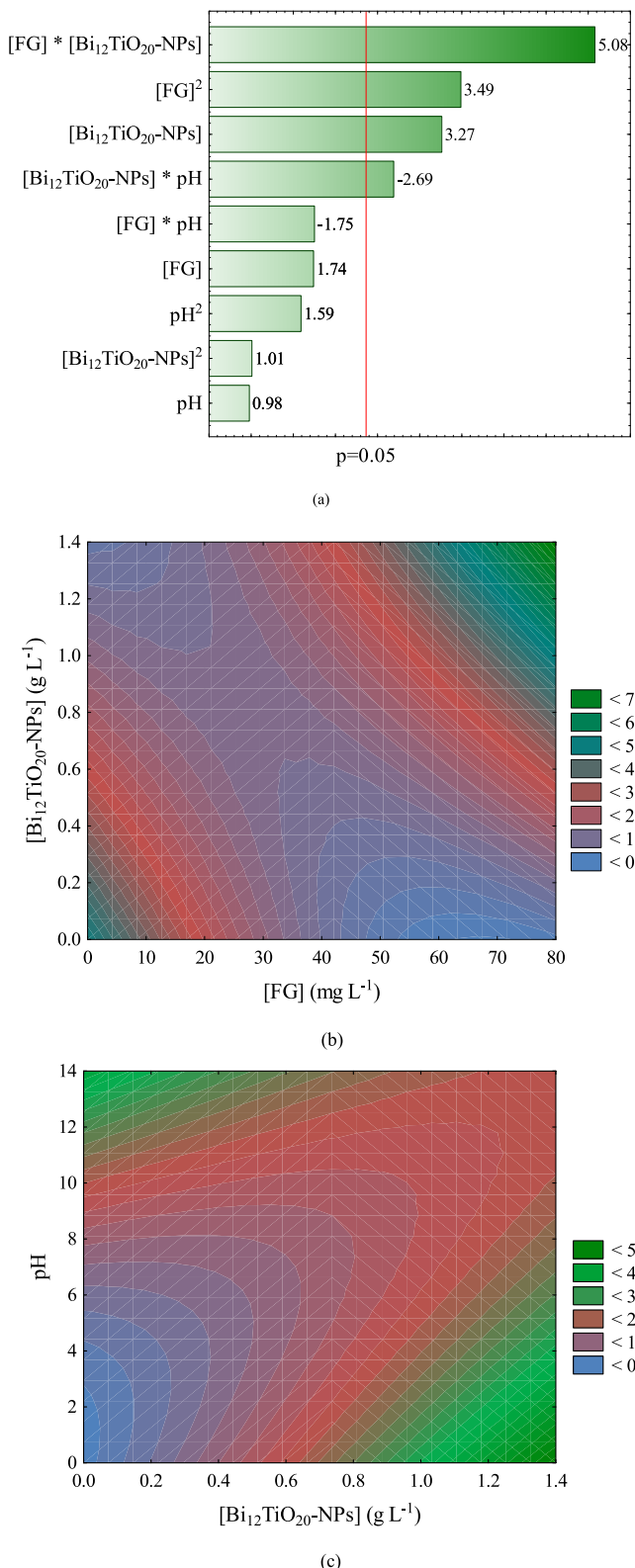


Fig. 5. (a) Pareto chart for the experimental design of FG dye degradation in the heterogeneous photocatalysis process; (b) 2D-surface for the FG photodegradation [$\text{Bi}_{12}\text{TiO}_{20}$ -NPs] and [FG]; and (c) -surface for the FG photodegradation [$\text{Bi}_{12}\text{TiO}_{20}$ -NPs] and pH.

Table 5

The sum of squares (SS), degrees of freedom (df), mean square error (MS), F_{cal} (calculated degrees of freedom), F_{tab} (degrees of freedom tabulated) and determination coefficient (R^2) for FG photodegradation.

	SS	df	MS	F_{cal}	F_{tab}	R^2
[FG]	50.33	1	50.33	24	3.68	0.90
[FG] ²	202.06	1	202.06			
pH	15.94	1	15.94			
pH ²	42.09	1	42.09			
[Bi ₁₂ TiO ₂₀ -NPs]	176.72	1	176.72			
[Bi ₁₂ TiO ₂₀ -NPs] ²	16.93	1	16.93			
[FG] * [Bi ₁₂ TiO ₂₀ -NPs]	428.18	1	428.18			
[FG] * pH	50.95	1	50.95			
[Bi ₁₂ TiO ₂₀ -NPs] * pH	120.31	1	120.31			
Error	115.96	7	16.57			
Total SS	1166.87	16	--			

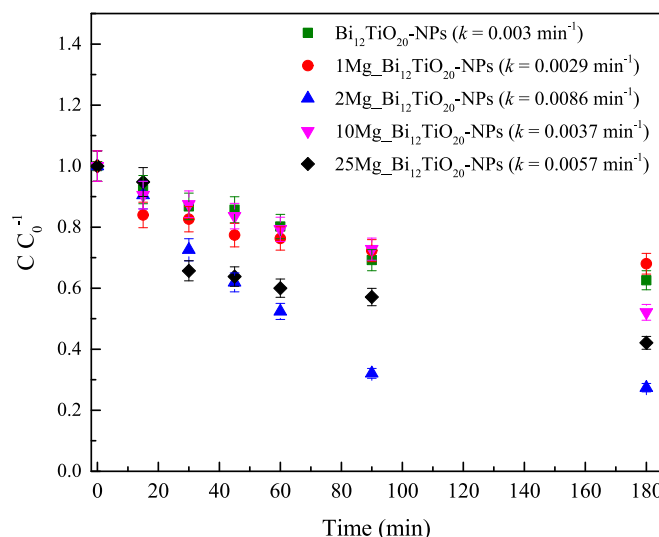


Fig. 6. Kinetic curve for the FG photodegradation under visible radiation utilizing Bi₁₂TiO₂₀-NPs and 1-25Mg_xBi₁₂TiO₂₀-NPs.

Bi₁₂TiO₂₀-NPs presented a type II isotherm (characteristic of the first adsorbed layer involving the entire Bi and Ti surface) and an H4 hysteresis curve associated with non-rigid aggregates of plate-shaped particles originated from aggregated pores with S_{BET} of $0.15 \pm 0.0001 \text{ m}^2 \text{ g}^{-1}$, V_p of $0.000665 \pm 0.0001 \text{ cm}^3 \text{ g}^{-1}$ and D_p of $41.74 \pm 0.8 \text{ nm}$ indicating a mesoporous material. It is worth mentioning that mesoporous materials facilitate the adsorption process of FG molecules and subsequently heterogeneous photocatalysis, aiding in the generation of oxidative radicals by redox reactions. However, Bi₁₂TiO₂₀-NPs was found in the literature with S_{BET} around $10-40 \text{ m}^2 \text{ g}^{-1}$ due to the temperatures of the thermal treatments used ($>873.15 \text{ K}$) occurring processes of coalescence, stabilization and particle growth [56,57].

Regarding the surface charge, Bi₁₂TiO₂₀-NPs presented a negative charge of $-0.32 \pm 0.02 \text{ mV}$ indicating compatibility charges with the FG (cationic) promoting greater diffusion and mass transfer from the absorbent to the surface of the adsorbent [42]. The effect of the surface charge of Bi₁₂TiO₂₀-NPs in Fig. 2(d) was investigated for evaluating the pH_{ZCP} using the 11-point assay. In this way, pH_{ZCP} of Bi₁₂TiO₂₀-NPs was approximately 6.18, indicating that when pH < pH_{ZCP} the surface of the nanocatalyst is protonated (+), while pH > pH_{ZCP} the surface is deprotonated (-) due the cationic dye (FG) natures a pH of around 6.0 will favor both photodegradation of the dyes by virtue of the increase of electrostatic interactions between the surface of Bi₁₂TiO₂₀-NPs and FG [58].

The band gap energy was evaluated using the Tauc plot method identified in Fig. 2(e), where Bi₁₂TiO₂₀-NPs showed $E_g = 2.24 \text{ eV}$

Table 6

Performance of the machine learning algorithms tested in this study.

Algorithm	Best configuration	Training R ²	Test R ²	Training RMSE	Training RMSE
DT	Min. sample splits: 10; Min. samples leaf: 1; and Max. tree depth: 3	0.9972	0.9671	0.6957	1.3887
RF	Max. tree depth: 10; Initial learning rate: 10%; Minimum samples leaf: 1; Minimum samples split: 2; and Number of decision trees: 100	0.9986	0.9676	0.5819	1.3840
KNN	Number of neighbors: 1; p = 1; and Weights: uniform	0.9999	0.8880	0.0126	1.8869
MLP-ANN	Batch size: 32; Early stopping: 120 of 200 epochs; Activation function: ReLU; Weight updating function: Adam; Patience of early stopping: 4; and Neural network architecture: 6:8:1	0.9977	0.9944	0.4273	0.7954

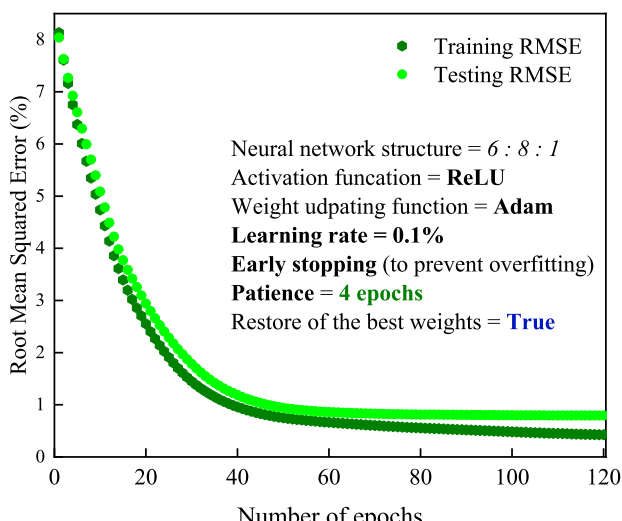
resulting in a displacement to the visible irradiation range increasing the applicability of the heterogeneous photocatalysis for solar radiation and facilitating the photoactivation of the Bi₁₂TiO₂₀-NPs due to the changes in the valence and conduction band through the quantum confinement effect [59]. Fig. 3 shows the FEG-SEM and SEM-EDX micrographs of Bi₁₂TiO₂₀-NPs and the particle size curve distribution.

In Fig. 3(a, c, d and e) it was possible to verify a rod and ellipses morphology with an average particle size of $88.9 \pm 24.8 \text{ nm}$ due to the calcination temperature (1073.15 K). Fig. 3(b) shows the elemental composition by EDX of the Bi₁₂TiO₂₀-NPs indicating a presence of oxygen (28.67 %), bismuth (38.63 %), and titanium (8.73 %). Thus, the Bi₁₂TiO₂₀-NPs biosynthesis was confirmed correlating the characterization techniques (XRD, FTIR, N₂ porosimetry, ZP and FEG-SEM). Fig. 4 shows the thermogravimetric analyze of the Bi₁₂TiO₂₀-NPs.

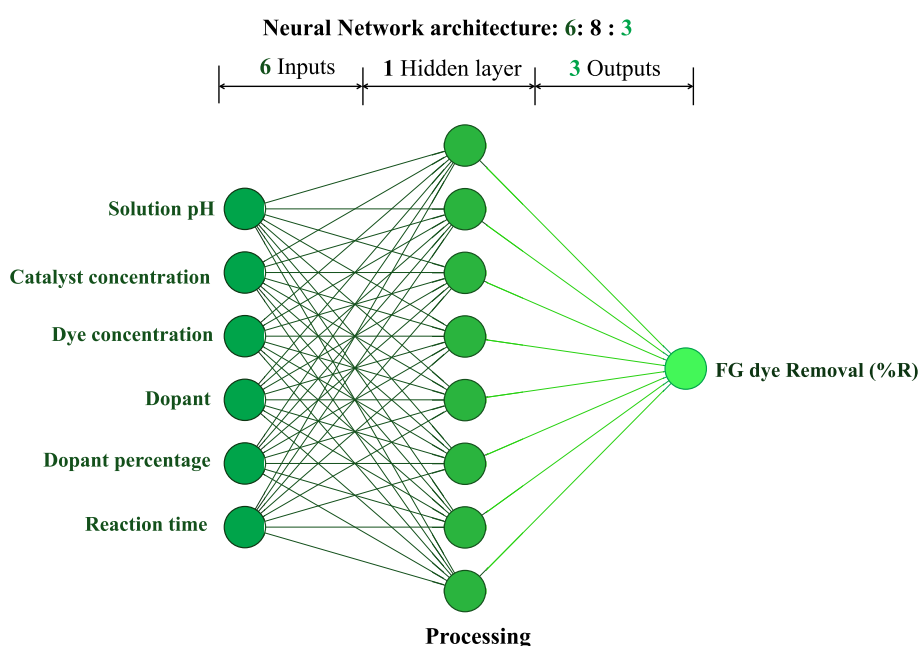
According to Fig. 4, Bi₁₂TiO₂₀-NPs demonstrated two mass losses in different ranges at temperatures from 525.5 K to 883.5 K associated with the degradation of carbonaceous materials (1.88 %) from the *M. officinalis* extract and degradation of inorganic components mainly titanium and bismuth groups (5.74 %), respectively [60]. It is noteworthy that the perovskite of titanium and bismuth showed high thermal stability and can be used in processes involving elevated temperatures.

3.3. Design experimental (CCRD 2³) and photocatalysis of FG

Table 4 shows the CCRD 2³ for FG photodegradation by heterogeneous photocatalysis, where the ideal condition denoted for heterogeneous photocatalysis was [FG] = 60 mg L⁻¹, [Bi₁₂TiO₂₀-NPs] = 1 g L⁻¹ and pH = 4 with 37.36 % of degradation. The ideal condition was used in the study of photodegradation kinetics of FG. Fig. 5(a-c) showed Pareto's chart and 2D response surfaces of the effects of independent variables on the photodegradation FG.



(a)



(b)

Fig. 7. (a) Learning profile of the MLP-ANN algorithm in the optimal configuration and (b) neural network architecture.

According to Fig. 5(a), the linear interaction of the dye concentration with the catalyst (5.08) exerted direct effects on the photodegradation of FG due to the processes of interaction and adsorption of molecules in the reaction medium, while [FG] represented a positive quadratic effect (3.49) on the photodegradation. Moreover, $[Bi_{12}TiO_{20}-NPs]$ demonstrates positive linear effect (3.27) in photodegradation in virtue to the increase in the number of active sites and generation of oxidative radicals. However, the interaction of $[Bi_{12}TiO_{20}-NPs]$ concentration and pH present a negative effect (-2.69) on photodegradation, generally associated with changes in charges in the nanocatalyst, reducing the initial stage of heterogeneous photocatalysis.

In relation to Table 5, where it was possible to demonstrate the main parameters since the F_{cal} (24) was four times greater than the F_{tab} (3.68) indicating that 90 % of the experimental data were adjusted in the model confirming the direct and indirect relationships of the independent

variables with the percentage of photodegradation of FG dye.

3.4. Photocatalytic assay

According to Fig. 6 the photodegradation of FG using $Bi_{12}TiO_{20}$ -NPs demonstrated a pseudo first order kinetics of 0.003 min^{-1} ($R^2 = 0.954$) with a removal of 37.36 % of FG after 180 min. It is noteworthy that the FG dye has a high molecular mass (808.9 g mol^{-1}) causing interparticle diffusion and mass transfer processes difficult resulting in a lower percentage of adsorption/photodegradation processes [61,62]. The effect of doping with $MgCl_2$ in the bismuth titanate nanocatalyst was possible to observe that there was an increase of about 36 % for 72.62 % of the FG removal ($k = 0.003\text{--}0.0086\text{ min}^{-1}$) when doped with 2 % w/w. It is noteworthy that $Bi_{12}TiO_{20}$ -NPs doped with 10 % and 25 % of Mg^{2+} decreased the percentage of FG photodegradation, due to the probable

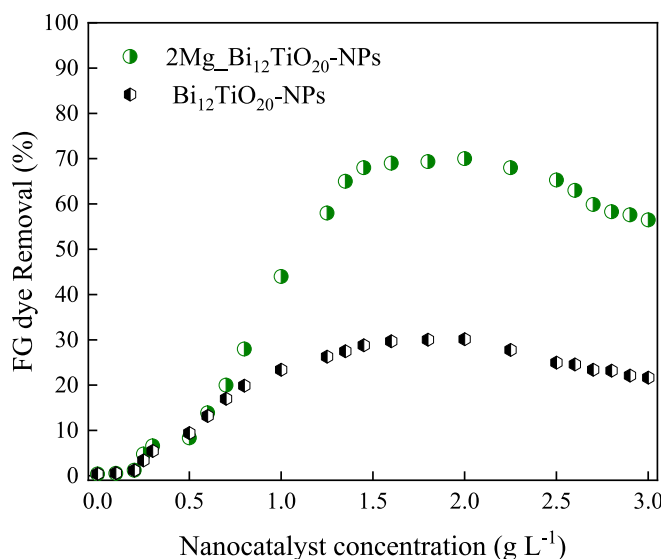


Fig. 8. Prediction of FG dye removal under visible light based on non-doped and magnesium-doped nanocatalyst concentrations using the ANN-MLP algorithm. (Operational parameters: 50 W | pH 4 | 298.15 ± 2 K | [FG] = 20 mg L⁻¹).

reduction in the number of catalytic active sites with the incorporation of MgO. A similar result/pattern is found in the literature [63].

3.5. Machine learning

Table 6 informs the model performance of each algorithm tested in the machine learning study used to predict FG dye removal for non-doped (Bi₁₂TiO₂₀-NPs) and doped nanocatalyst (2Mg_xBi₁₂TiO₂₀-NPs) within and beyond the experimental set used in this work.

According to Table 6, the neural network (MLP-ANN) showed the best performance ($R^2 \sim 0.9999$ and lowest RMSE values) among the machine learning algorithms. Although the satisfactory performance of DT, RF and KNN, these algorithms resulted in RMSE being higher than MLP-ANN. Then, the MLP-ANN algorithm was selected to develop a generic predictive model. Moreover, the proximity between the RMSE values for training and testing data in the MLP-ANN algorithm indicates a good ability of the model to perform generalizations and a low probability of overfitting [64]. Fig. 7 shows the learning profile for the training and testing dataset.

Fig. 8 demonstrates the predicted removal efficiency of FG dye under visible light as a function of nanocatalyst concentration for both magnesium-doped (2Mg_xBi₁₂TiO₂₀-NPs) and non-doped (Bi₁₂TiO₂₀-NPs) nanocatalysts. These predictions were performed for concentrations within and beyond the experimental set design for this work.

According to Fig. 8, the predictions reveal a clear enhancement in the performance of the doped nanocatalyst. For the magnesium-doped variant, the removal efficiency increases sharply with concentration, reaching a maximum near to 70 % before declining slightly at higher concentrations. In contrast, the non-doped nanocatalyst exhibits a slower increase in removal efficiency up to 30 % and plateauing thereafter.

These differences underscore the significant role of magnesium

doping in improving the photocatalytic activity by enhancing light absorption and charge carrier separation, which are critical for efficient dye degradation. Thus, at 2.0 g L⁻¹, a maximum of 30 % dye removal is achieved with the non-doped nanocatalyst (Bi₁₂TiO₂₀-NPs), whereas a maximum of 70 % is achieved when the magnesium-doped nanocatalyst (2Mg_xBi₁₂TiO₂₀-NPs) is used.

Therefore, the doped nanocatalyst consistently outperforms the non-doped variant, with higher predicted efficiencies at both low and high concentrations, emphasizing the critical role of magnesium in improving the photocatalytic performance of the nanocatalyst. Moreover, a similar tendency was observed in the literature [65,66].

Table 7 shows a comparative study of nanoparticles used in the photodegradation of different pollutants based on ANN models.

As presented in Table 7, the determination coefficient (R^2) of the MLP-ANN model used in this study presented values in the range of previous studies using a similar number of parameters in input and output layers, and neurons in the hidden layers. Therefore, the results showed that the MLP-ANN model was effective in predicting values of removal of FG by photodegradation using the Bi₁₂TiO₂₀-NPs nanocatalyst, justifying its novelty based on the use of open-source software.

3.6. Bi₁₂TiO₂₀-NPs, and 2Mg_xBi₁₂TiO₂₀-NPs phytotoxicity

Fig. 9(a-b) show the phytotoxicity results of the Bi₁₂TiO₂₀-NPs and 2Mg_xBi₁₂TiO₂₀-NPs on *Lactuca Sativa* and *Daucus carota* seeds after 78 h, where the concentration in 10 mg L⁻¹ of the nanoparticles showed around of 50 % inhibition in the root radicular growth of both seeds possibly due to the small number of functional groups (Ti-O and Bi-O) [70]. Moreover, the increase in root radicular growth (around 40 %) of *Lactuca Sativa* and *Daucus carota* seeds containing the 2Mg_xBi₁₂TiO₂₀-NPs in elevated concentrations is possibly related to the increase in electrical conductivity, being a limiting factor exerting direct effects on the water absorption. Water retention capacity, water consumption, division and cell growth of roots, moisture content, nutrient absorption and electrical conductivity are effects dependent on the type of seed related to interactions with nanoparticles, being the *Lactuca Sativa* seed sensitive to any change in the medium denoted in the results of phytotoxicity [71]. Thus, the doping with Mg²⁺ ions on Bi₁₂TiO₂₀-NPs is a promising green nanocatalyst for applications in ecotoxicity.

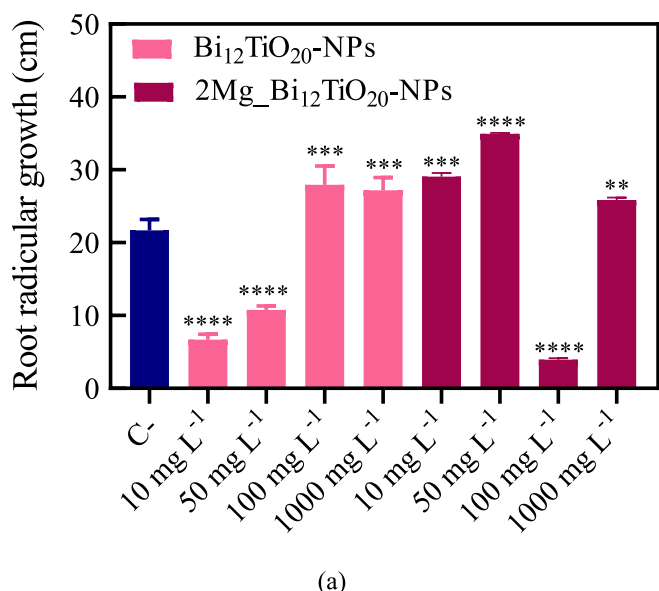
4. Conclusion

This study investigated the application of Bi₁₂TiO₂₀-NPs and magnesium-doped (2Mg_xBi₁₂TiO₂₀-NPs) nanocatalysts for the photodegradation of Fast Green (FG) dye under visible light. The characterization of the nanocatalysts, performed by techniques such as XRD, FTIR, N₂ porosimetry, ZP and SEM, revealed that the materials presented nanometric morphology, with good thermal stability and promising photocatalytic properties. The presence of the magnesium dopant in Bi₁₂TiO₂₀-NPs was crucial to improve the photodegradation efficiency of the FG dye, demonstrating a significant increase in the removal efficiency, reaching 70 % at 2.0 g L⁻¹, compared to 30 % obtained with the undoped nanocatalyst. The predictive modeling of FG removal using the MLP-ANN neural network proved to be highly effective, presenting a coefficient of determination (R²) close to 0.9999 and low RMSE values, highlighting the model's ability to generalize and accurately predict experimental data. The comparison between the machine learning

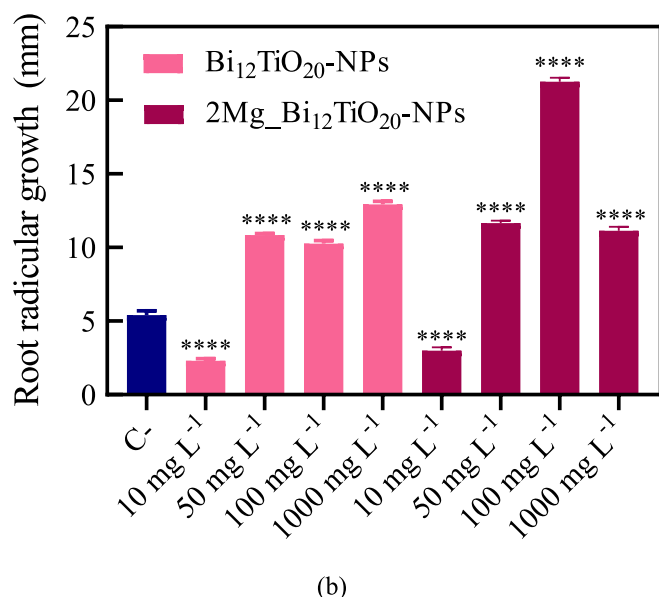
Table 7

Nanocatalysts are used in heterogeneous photodegradation of pollutants based on ANN models.

Pollutant	Nanocatalyst	ANN structure	Metrics	Reference
Brilliant Blue FCF	ZnO	(5:9:1)	$R^2 = 0.9883$, RMSE = 0.0242	[67]
Methylene blue	BiVO ₄ /BiPO ₄ /rGO	(4:11:1)	$R^2 = 0.9838$	[68]
4-Nonylphenol	TiO ₂	(4:14:1)	$R^2 = 0.9925$	[69]
Fast Green	Bi ₁₂ TiO ₂₀ -NPs	(6:8:1)	$R^2 = 0.9977$, RMSE = 0.4273	This study



(a)



(b)

Fig. 9. (a) Root radicular growth of *Lactuca Sativa* seeds and (b) root radicular growth of *Daucus carota* seeds after 78 h of samples with significant values; (*) $p < 0.05$, (**) $p < 0.01$, (***) $p < 0.001$ and (****) $p < 0.0001$.

models (MLP-ANN, DT, RF and KNN) demonstrated that MLP-ANN outperformed the others, with the best performance for both training and testing data, confirming its applicability in photocatalytic systems. In addition, the phytotoxicity analysis of the nanocatalysts, performed with *Lactuca sativa* and *Daucus carota* seeds, indicated that concentrations of 10 mg L^{-1} of the nanocatalysts caused approximately 50 % inhibition of root growth, with a distinct response to the magnesium dopant. The magnesium-doped nanocatalyst ($2\text{Mg}_-\text{Bi}_{12}\text{TiO}_{20}\text{-NPs}$) promoted an increase in seed root growth at high concentrations, possibly due to the higher electrical conductivity and interaction with the nanoparticles. These results suggest that Mg^{2+} doping is an effective strategy to improve the photocatalytic and ecological properties of nanocatalysts, highlighting their potential for applications in environmental processes, such as pollutant degradation. Therefore, it was possible to integrate nanotechnology and artificial intelligence to develop a potential eco-friendly nanomaterial for application in the

treatment of wastewater with dyes through heterogeneous photocatalysis.

Ethical approval

Not applicable to this work.

Consent to participate

Not applicable.

Consent to publish

All authors read and approved of the final manuscript.

Availability of data and materials

The Python codes used to build the models, raw data used in this study, model stable test results, and GUI application code are available at the following GitHub link (<https://github.com/LeandroOviedo/Machine-and-Deep-Learning>).

CRedit authorship contribution statement

Sth  fany Nunes Loureiro: Writing – review & editing, Writing – original draft, Validation, Investigation, Formal analysis, Data curation, Conceptualization. **Daniel Moro Druzian:** Writing – review & editing, Data curation, Conceptualization. **Leandro Rodrigues Oviedo:** Writing – review & editing, Writing – original draft, Data curation, Conceptualization. **Cristiane dos Santos:** Writing – review & editing, Writing – original draft, Conceptualization. **Yolice Patricia Moreno Ruiz:** Writing – review & editing, Data curation, Conceptualization. **Andr   Galembeck:** Writing – review & editing, Data curation, Conceptualization. **Giovani Pavoski:** Writing – review & editing, Formal analysis, Conceptualization. **Jorge Alberto Soares Ten  rio:** Conceptualization, Formal analysis, Writing – review & editing. **Denise Crocce Romano Espinosa:** Writing – review & editing, Formal analysis, Conceptualization. **William Leonardo da Silva:** Writing – review & editing, Writing – original draft, Validation, Supervision, Investigation, Formal analysis, Data curation, Conceptualization.

Funding

Our research group appreciates the financial support provided by the Conselho Nacional de Desenvolvimento Cient  fico e Tecnol  gico (CNPq / PIBIC 17/2023) for assistance and financial support.

Declaration of competing interest

The authors declare that they have no known competing financial interests or personal relationships that could have appeared to influence the work reported in this paper.

Acknowledgments

Department of Fundamental Chemistry at Federal University of Pernambuco (UFPE), University of Sao Paulo (LAREX USP, Brazil – SP) and Franciscan University (UFN, Brazil – RS) for the support and assistance to carry out the present work.

Data availability

Data will be made available on request.

References

- [1] S. Mohanty, S. Moulick, S.K. Maji, Adsorption/photodegradation of crystal violet (basic dye) from aqueous solution by hydrothermally synthesized titanate nanotube (TNT), *J. Water Process Eng.* 37 (2020) 101428–101437, <https://doi.org/10.1016/j.jwpe.2020.101428>.
- [2] N.V. Mdlovu, N.-C. Yang, K.-S. Lin, C.-J. Chang, K.T. Dinh, Y.-G. Lin, Formulation and characterization of W-doped titania nanotubes for adsorption/photodegradation of methylene blue and basic violet 3 dyes, *Catal. Today* 388–389 (2022) 36–46, <https://doi.org/10.1016/j.cattod.2021.03.015>.
- [3] Z.Z. Vasiljevic, M.P. Dojcinovic, J.D. Vujsancevic, I. Jankovic-Castvan, M. Ognjanovic, N.B. Tadic, S. Stojadinovic, G.O. Brankovic, M.V. Nikolic, Photocatalytic degradation of methylene blue under natural sunlight using iron titanate nanoparticles prepared by a modified sol-gel method, *Royal Soc. Open Sci.* 7 (2020) 200708–200722, <https://doi.org/10.1098/rsos.200708>.
- [4] M.A. Adelin, G. Gunawan, M. Nur, A. Haris, D.S. Widodo, L. Suyati, Ozonation of methylene blue and its fate study using LCMS/MS, *J. Phys. Conf. Ser.* 1524 (2020) 012079–012089, <https://doi.org/10.1088/1742-6596/1524/1/012079>.
- [5] R. Sadraei, Fast, green and easy adsorption of dye and emerging contaminants by functionalized γ -AACH, *J. Environ. Chem. Eng.* 8 (2020) 103616–103625, <https://doi.org/10.1016/j.jece.2019.103616>.
- [6] A. Kumar, M. Paliwal, R. Ameta, S.C. Ameta, Oxidation of fast green FCF by the solar photo-Fenton process, *J. Iran. Chem. Soc.* 5 (2008) 346–351, <https://doi.org/10.1007/bf0324612>.
- [7] M. Nazim, A.A.P. Khan, A.M. Asiri, J.H. Kim, Exploring rapid photocatalytic degradation of organic pollutants with porous CuO nanosheets: synthesis, dye removal, and kinetic studies at room temperature, *ACS Omega* 6 (2021) 2601–2612, <https://doi.org/10.1021/acsomega.0c04747>.
- [8] S. Lim, J.L. Shi, U. Gunten, D.L. McCurry, Ozonation of organic compounds in water and wastewater: A critical review, *Water Res.* 213 (2022) 118053–118086, <https://doi.org/10.1016/j.watres.2022.118053>.
- [9] D. Friedmann, A general overview of heterogeneous photocatalysis as a remediation technology for wastewaters containing pharmaceutical compounds, *Water* 14 (2022) 3588–3619, <https://doi.org/10.3390/w14213588>.
- [10] S. He, Y. Chen, X. Li, L. Zeng, M. Zhu, Heterogeneous photocatalytic activation of persulfate for the removal of organic contaminants in water: A critical review, *ACS EST Eng.* 2 (2022) 527–546, <https://doi.org/10.1021/acsestengg.1c0033>.
- [11] Z. Ajmal, M.U. Haq, S. Zaman, M.K. Al-Muhanna, A. Kumar, M.M. Fahdali, S.B. H. Hassine, M. Qasim, K.F. Alshammari, G.A. Ashraf, A. Qadeer, A. Murtaza, S. Al-Sulaimi, H. Zeng, Addressing the synchronized impact of a novel strontium titanium over copolymerized carbon nitride for proficient solar-driven hydrogen evolution, *J. Colloid Interf. Sci.* 655 (2024) 886–898, <https://doi.org/10.1016/j.jcis.2023.10.020>.
- [12] J. Ye, T.K. Banda, Z. Ajmal, J. Ahmed, S. Raza, E. Ghasali, A. Hayat, Y. Orooji, Organic conjugation of graphitic carbon nitride nanocomposites for boosted photocatalytic water splitting, *Mat. Sci. Semicon. Proc.* 166 (2023) 107742, <https://doi.org/10.1016/j.mssp.2023.107742>.
- [13] H. Ali, Z. Ajmal, I. Boukhri, A.M. Alenad, M.S. Al-Buraihi, A.M. Abu-Dief, N. S. Alsaiari, A. Hayat, H.M.A. Hassan, Y. Liang, D. Yue, Recent advances, synthesis, modifications and photogenerated carrier dynamics of g-C₃N₄ for photocatalytic water splitting, *Int. J. Hydrogen Energ.* 100 (2025) 79–128, <https://doi.org/10.1016/j.ijhydene.2024.12.181>.
- [14] Z. Ajmal, A. Hayat, M. Qasim, A. Kumar, A.E. Jery, W. Abbas, M.B. Hussain, A. Qadeer, S. Iqbal, S. Bashir, Z. Ahmad, J. Qian, A. Murtaza, H. Zeng, Assembly of a novel Fe₂TiO₅-impregnated donor- π -acceptor conjugated carbon nitride for highly efficient solar water splitting, *Sustain. Mater. Technol.* 36 (2023) e00594, <https://doi.org/10.1016/j.susmat.2023.e00594>.
- [15] Z. Ajmal, T.A. Taha, M.A. Amin, A. Palamanit, W.I. Nawawi, A. Kalam, A.G. Al-Shehmi, H. Algarni, A. Qadeer, H. Ali, A. Kumar, J. Qian, A. Hayat, H. Zeng, Embedding aromatic conjugated monomer within carbon nitride for efficient photocatalytic reduction reactions, *J. Mol. Liq.* 368 (2022) 120617, <https://doi.org/10.1016/j.molliq.2022.120617>.
- [16] Z. Ajmal, H. Ali, S. Ullah, A. Kumar, M. Abboud, H. Gul, Y. Al-Hadeethi, A. S. Alshammari, N. Almuqati, G.A. Ashraf, N. Hassan, A. Qadeer, A. Hayat, M. U. Haq, I. Hussain, A. Murtaza, Use of carbon-based advanced materials for energy conversion and storage applications: Recent Development and Future Outlook, *Fuel* 367 (2024) 131295, <https://doi.org/10.1016/j.fuel.2024.131295>.
- [17] Z. Ajmal, M. Arif, A. Kumar, M.U. Haq, Y. Du, Y. Zhang, M. Abboud, J. Qian, Z. Chen, B.-J. Ni, H. Zeng, Uniformly distributed Ru nanoparticles over N, P codoped porous carbon as a highly active trifunctional electrocatalyst, *Int. J. Hydrogen Energ.* 73 (2024) 768–774, <https://doi.org/10.1016/j.ijhydene.2024.05.451>.
- [18] M.H. Abdel-Razak, M. Emam, S. Ookawara, H. Hassan, Power performance enhancement for a three-turbine cluster of two-stage Savonius rotors using Taguchi approach, *Energy* 308 (2024) 132903, <https://doi.org/10.1016/j.energy.2024.132903>.
- [19] Z. Ajmal, A. Hayat, A. Qadeer, Y. Zhao, E.H. Ibrahim, M.U. Haq, K. Iqbal, M. Imran, M. Kuku, I. Hussain, H. Ali, Y. Orooji, J.L. Zhou, T. Ben, Advancements in MXene-based frameworks towards photocatalytic hydrogen production, carbon dioxide reduction and pollutant degradation: Current challenges and future prospects, *Coordin. Chem. Rev.* 523 (2025) 216226, <https://doi.org/10.1016/j.ccr.2024.216226>.
- [20] A. Hayat, Z. Ajmal, A.Y.A. Alzahrani, S.B. Moussa, M. Khered, N. Almuqati, A. Alshammari, Y. Al-Hadeethi, H. Ali, Y. Orooji, The photocatalytic H₂O₂ production: Design strategies, Photocatalyst advancements, environmental applications and future prospects, *Coordin. Chem. Rev.* 522 (2025) 216218, <https://doi.org/10.1016/j.ccr.2024.216218>.
- [21] V.H. Rath, A.R. Jeice, Green fabrication of titanium dioxide nanoparticles and their applications in photocatalytic dye degradation and microbial activities, *Chem. Phys. Impact* 6 (2023) 100197–100210, <https://doi.org/10.1016/j.chphi.2023.100197>.
- [22] M. Coto, S.C. Troughton, P. Knight, R. Joshi, R. Francis, R.V. Kumar, T.W. Clyne, Optimization of the microstructure of TiO₂ photocatalytic surfaces created by Plasma Electrolytic Oxidation of titanium substrates, *Surf. Coat. Technol.* 411 (2021) 127000–127011, <https://doi.org/10.1016/j.surfcoat.2021.127000>.
- [23] J. Shi, W. Fu, Y. Jiang, B. Wang, H. Liu, W. Ji, Z. Wang, Chen, Construction of g-C₃N₄/Bi₄Ti₃O₁₂ hollow nanofibers with highly efficient visible-light-driven photocatalytic performance, *Colloids Surf. A: Physicochem. Eng.* 615 (2021) 126063–126074, <https://doi.org/10.1016/j.colsurfa.2020.126063>.
- [24] A. Shafiee, M. Baneshti, R.S. Varma, E. Mostafavi, S. Iravani, Biosynthesized metallic nanocatalysts in the removal and degradation of pollutants, *Mater. Lett.* 326 (2022) 132911–132917, <https://doi.org/10.1016/j.matlet.2022.132911>.
- [25] N. Motakef-Kazemi, M. Yaqoubi, Green synthesis and characterization of bismuth oxide nanoparticle using Mentha Pulegium Extract, *Iran. J. Pharm. Res.* 19 (2020) 70–79, <https://doi.org/10.22037/ijpr.2019.15578.13190>.
- [26] E.T. Bekele, B.A. Gonfa, O.A. Zeleke, H.H. Belay, F.K. Sabir, Synthesis of titanium oxide nanoparticles using root extract of *Kniphofia foliosa* as a template, characterization, and its application on drug resistance bacteria, *J. Nanomater.* 1 (2020) 2817037–2817047, <https://doi.org/10.1155/2020/2817037>.
- [27] M. Alagawany, M.E.A. El-Hack, M.R. Farag, M. Gopi, K. Karthik, Y.S. Malik, K. Dhama, Rosmarinic acid: Modes of action, medicinal values, and health benefits, *Anim. Health Res. Rev.* 18 (2017) 167–176, <https://doi.org/10.1017/S1466252317000081>.
- [28] A. Asadi, F. Shidfar, M. Safari, M. Malek, A.F. Hosseini, S. Rezazadeh, A. Rajab, S. Shidfar, S. Hosseini, Safety, and efficacy of *Melissa officinalis* (lemon balm) on ApoA-I, Apo B, lipid ratio and ICAM-1 in type 2 diabetes patients: A randomized, double-blinded clinical trial, *Complement. Ther. Med.* 40 (2018) 83–88, <https://doi.org/10.1016/j.ctim.2018.07.015>.
- [29] C. Yaman, Lemon balm and sage herbal teas: Quantity and infusion time on the benefit of the content, *Food Sci. Technol.* 44 (2020) 023220–023231, <https://doi.org/10.1590/1413-705420244023220>.
- [30] Y. Chen, C. Zhao, W. Tan, S. Gong, H. Pan, X. Liu, S. Huang, Q. Shi, Visible light-driven copper vanadate/biochar nanocomposite for heterogeneous photocatalysis degradation of tetracycline: Performance, mechanism, and application of machine learning, *Environ. Res.* 267 (2025) 120747–120759, <https://doi.org/10.1016/j.envres.2024.120747>.
- [31] Z.H. Jaffari, A. Abbas, C.-M. Kim, J. Shin, J. Kwak, C. Son, Y.-G. Lee, S. Kim, K. Chon, K.H. Cho, Transformer-based deep learning models for adsorption capacity prediction of heavy metal ions toward biochar-based adsorbents, *J. Hazard. Mater.* 462 (2024) 132773–132785, <https://doi.org/10.1016/j.jhazmat.2023.132773>.
- [32] M. Motamed, L. Yerushalmi, F. Haghighe, Z. Chen, Y. Zhuang, Comparison of photocatalysis and photolysis of 2,2,4,4-tetrabromodiphenyl ether (BDE-47): Operational parameters, kinetic studies, and data validation using three modern machine learning models, *Chemosphere* 326 (2023) 138363–138372, <https://doi.org/10.1016/j.chemosphere.2023.138363>.
- [33] X. Li, X. Zhang, J. Zhang, J. Gu, S. Zhang, G. Li, J. Shao, Y. He, H. Yang, S. Zhang, H. Chen, Applied machine learning to analyze and predict CO₂ adsorption behavior of metal-organic frameworks, *Carbon Capture Sci. Technol.* 9 (2023) 100146–100155, <https://doi.org/10.1016/j.cscst.2023.100146>.
- [34] A.J. Ruiz-Baltazar, S.Y. Reyes-López, D. Larrañaga, M. Estévez, R. Pérez, Green synthesis of silver nanoparticles using a *Melissa officinalis* leaf extract with antibacterial properties, *Results Phys.* 7 (2017) 2639–2643, <https://doi.org/10.1016/j.rinp.2017.07.044>.
- [35] C.C. Silva, M.P.F. Graça, M.A. Valente, A.S.B. Sombra, Crystallite size study of nanocrystalline hydroxyapatite and ceramic system with titanium oxide obtained by dry Ball milling, *J. Mater. Sci.* 42 (2007) 3851–3855, <https://doi.org/10.1007/s10853-006-0474-0>.
- [36] C. Rosa, F. Auriemma, *Crystals and Crystallinity in Polymers: Diffraction Analysis of Ordered and Disordered Crystals*, fourth ed., Elsevier, England, 2014.
- [37] M. Thommes, K. Kaneko, A.V. Neimark, J.P. Olivier, F.R. Reinoso, J. Rouquerol, K. S.W. Sing, Physisorption of gases, with special reference to the evaluation of surface area and pore size distribution (IUPAC Technical Report), *Pure Appl. Chem.* 87 (2015) 1051–1069, <https://doi.org/10.1515/pac-2014-1117>.
- [38] F.I.A. El-Fadil, A.M. Elbarbary, Radiation synthesis and characterization of heterogeneous magnetic nanocomposites of 2-hydroxyethyl methacrylate for catalytic degradation of Sandocryl Blue dye, *Sep. Purif. Technol.* 272 (2021) 118972–118986, <https://doi.org/10.1016/j.seppur.2021.118972>.
- [39] A. Jacobson, C. Chen, J. Dewey, G. Copeland, W. Allen, B. Richards, J.D. Kaszuba, A. van Duin, H. Cho, M. Deo, Y. She, T. Martin, Effect of nanoconfinement and pore geometry on point of zero charge in synthesized mesoporous siliceous materials, *JCIS Open* 8 (2022) 100069–100079, <https://doi.org/10.1016/j.jciso.2022.100069>.
- [40] I. Bhati, P.B. Punjabi, S. Ameta, Photocatalytic degradation of fast green using nanosized CeCrO₃, *Maced. J. Chem. Chem.* 29 (2010) 195–202, <https://doi.org/10.20450/mjccc.2010.166>.
- [41] P.R. Gogate, A.B. Pandit, A review of imperative technologies for wastewater treatment I: oxidation technologies at ambient conditions, *Adv. Environ. Res.* 8 (2004) 501–515, [https://doi.org/10.1016/S1093-0191\(03\)00032-7](https://doi.org/10.1016/S1093-0191(03)00032-7).
- [42] U.I. Gayà, A.H. Abdullah, Heterogeneous photocatalytic degradation of organic contaminants over titanium dioxide: a review of fundamentals, progress and

- problems, *J. Photochem. Photobiol. C* 9 (2008) 1–12, <https://doi.org/10.1016/j.jphotochemrev.2007.12.003>.
- [43] C. Zhang, S.N. Oliaee, S.Y. Hwang, X. Kong, Z. Peng, A generic wet impregnation method for preparing substrate-supported platinum group metal and alloy nanoparticles with controlled particle morphology, *Nano Lett.* 16 (2016) 164–169, <https://doi.org/10.1021/acs.nanolett.5b04518>.
- [44] W.L. Silva, M.A. Lansarin, Synthesis, characterization and photocatalytic activity of nanostructured TiO₂ catalysts doped with metals, *Quím. Nova.* 36 (2013) 382–386, <https://doi.org/10.1590/S0100-40422013000300006>.
- [45] W.L. Da-Silva, M.A. Lansarin, J.H.Z. Dos-Santos, F. Silveira, Photocatalytic degradation of rhodamine B, paracetamol and diclofenac sodium by supported titania-based catalysts from petrochemical residue: effect of doping with magnesium, *Water Sci. Technol.* 74 (2016) 2370–2383, <https://doi.org/10.2166/wst.2016.362>.
- [46] A. Falanga, A. Siciliano, M. Vitiello, G. Franci, V.D. Genio, S. Galdiero, M. Guida, F. Carraturo, A. Fahmi, E. Galdiero, Ecotoxicity evaluation of pristine and indolicidin-coated silver nanoparticles in aquatic and terrestrial ecosystem, *Int. J. Nanomed.* 15 (2020) 8097–8108, <https://doi.org/10.2147/ijn.s260396>.
- [47] C. Vieira, C. Marcon, A. Drosté, Phytotoxic and cytogenotoxic assessment of glyphosate on *Lactuca sativa* L. *Braz. J. Biol.* 84 (2024) e257039e-e, <https://doi.org/10.1590/1519-6984.257039>.
- [48] A. El Bey, M. Laidi, A. Yettu, A. Hanini, A. Ibrir, M. Bentabli, H. Ouldkhaoua, Practical artificial neural network tool for predicting the competitive adsorption of dyes on gemini polymeric nanoarchitecture, *Kem. Ind.* 70 (2021) 481–488, <https://doi.org/10.15255/KUL.2020.069>.
- [49] D.P. Kingma, J.L. Ba, Adam: A method for stochastic optimization (version 9), 3rd International Conference for Learning Representations, San Diego, 2015. doi: 10.48550/arXiv.1412.6980.
- [50] J. Li, L. Pan, M. Suvarna, Y.W. Tong, X. Wang, Fuel properties of hydrochar and pyrochar: Prediction and exploration with machine learning, *Appl. Energy* 269 (2020) 115166–115175, <https://doi.org/10.1016/j.apenergy.2020.115166>.
- [51] X. Yuan, M. Survana, S. Low, P.D. Dissanayake, K.B. Lee, J. Li, X. Wang, Y.S. Ok, Applied machine learning for prediction of CO₂ adsorption on biomass waste-derived porous carbons, *Environ. Sci. Tech.* 55 (2021) 11925–11936, <https://doi.org/10.1021/acs.est.1c01849>.
- [52] C. Caleja, L. Barros, M.A. Prieto, M.F. Barreiro, M.B.P.P. Oliveira, S.C.F.R. Ferreira, Extraction of rosmarinic acid from *Melissa officinalis* L. by heat-, microwave- and ultrasound-assisted extraction techniques: A comparative study through response surface analysis, *Sep. Purif. Technol.* 186 (2017) 297–308, <https://doi.org/10.1016/j.seppur.2017.06.029>.
- [53] M.T.L.P. Peres, J.R.R. Lopes, C.B. da Silva, A.C.S. Cândido, E. Simionatto, M.R. P. Cabral, R.M. Oliveira, J.T. Facco, C.A.L. Cardoso, P.H. Simas, Phytotoxic and antioxidant activity of seven native fruits of Brazil, *Acta Bot. Bras.* 27 (2013) 836–846, <https://doi.org/10.1590/0010-23062013000400024>.
- [54] M. Kireva, V. Tumbalev, Rietveld study of the changes of phase composition, crystal structure, and morphology of BiFeO₃ by partial substitution of bismuth with rare-earth ions, *Minerals* 11 (2021) 278–289, <https://doi.org/10.3390/min11030278>.
- [55] X. Liu, Z. Zhou, D. Han, T. Wang, C. Ma, P. Huo, Y. Yan, Interface engineered 2D/2D Ni(OH)₂/Bi₄Ti₃O₁₂ nanocomposites with higher charge transfer towards improving photocatalytic activity, *J. Alloy. Compd.* 816 (2019) 152530–152538, <https://doi.org/10.1016/j.jallcom.2019.152530>.
- [56] X. Yu, X. Zhang, J. Zhao, L. Xu, J. Yan, Flower-like shaped Bi₁₂TiO₂₀/g-C₃N₄ heterojunction for effective elimination of organic pollutants: Preparation, characterization, and mechanism study, *Appl. Organomet. Chem.* 34 (2020) 1–13, <https://doi.org/10.1002/aoc.5700.1002/aoc.5702>.
- [57] N.U.M. Nizam, M.M. Hanafiah, E. Mahmoudi, A.A. Halim, A.W. Mohammad, The removal of anionic and cationic dyes from an aqueous solution using biomass-based activated carbon, *Sci. Rep.* 11 (2021) 8623–8630, <https://doi.org/10.1038/s41598-021-88084-z>.
- [58] A. Stavrinou, C.A. Aggelopoulos, C.D. Tsakiroglou, Exploring the adsorption mechanisms of cationic and anionic dyes onto agricultural waste peels of banana, cucumber and potato: Adsorption kinetics and equilibrium isotherms as a tool, *J. Environ. Chem. Eng.* 6 (2018) 6958–6970, <https://doi.org/10.1016/j.jece.2018.10.063>.
- [59] T. Zhang, C. Hu, J. Wu, B. Shen, S. Peng, Y. Qi, M. Tao, X. Mao, Y. Tao, Y. Wang, Fabrication, structure, and application of sulfur- and sulfide-modified bismuth based photocatalysts: A review, *Separat. Purificat. Technol.* 323 (2023) 124352–124359, <https://doi.org/10.1016/j.seppur.2023.124352>.
- [60] Q. Xu, S. Xie, F. Wang, J. Liu, J. Shi, J. Xing, Q. Chen, J. Zhu, Q. Wang, Bismuth titanate based piezoceramics: Structural evolutions and electrical behaviors at different sintering temperatures, *J. Alloy. Compd.* 882 (2021) 160637–160648, <https://doi.org/10.1016/j.jallcom.2021.160637>.
- [61] G.R. Vaz, A. Clementino, J. Bidone, M.A. Villetti, M. Falkembach, M. Batista, P. Barros, F. Sonvico, C. Dora, Curcumin and quercetin-loaded nanoemulsions: physicochemical compatibility study and validation of a simultaneous quantification method, *Nanomaterials* 10 (2020) 1650–1669, <https://doi.org/10.3390/nano10091650>.
- [62] H.D. Tran, D.Q. Nguyen, P.T. Do, U.N.P. Tran, Kinetics of photocatalytic degradation of organic compounds: a mini-review and new approach, *RSC Adv.* 25 (2023) 16915–16925, <https://doi.org/10.1039/d3ra01970>.
- [63] P. Meenakshi, M. Pavithra, A.K.N. Pavithra, M. Salvaraj, Investigation on infrared reflective property of Mg-doped bismuth titanate for the application of cool home coating, *Int. J. Res. Advent. Technol.* 6 (2018) 2136–2144, <https://doi.org/10.32622/ijrat>.
- [64] L.R. Oviedo, V.R. Oviedo, L.D.D. Nora, W.L. Da Silva, Adsorption of organic dyes onto nanozeolites: A machine learning study, *Sep. Purif. Technol.* 315 (2023) 123712–123719, <https://doi.org/10.1016/j.seppur.2023.123712>.
- [65] R. Wang, C. Chu, L. Wang, Q. Liu, Investigation of the photocatalytic performance of Mg-doped modified BiOCl, *Inorg. Chem. Commun.* 157 (2023) 111286, <https://doi.org/10.1016/j.inoche.2023.111286>.
- [66] T. Zhao, Z. Ye, M. Zeng, W. Li, W. Luo, Q. Xiao, J. Xu, Molten salt synthesis of Mg-doped Ta₃N₅ nanoparticles with optimized surface properties for enhanced photocatalytic hydrogen evolution, *Energy Fuels* 37 (2023) 18194–18203, <https://doi.org/10.1021/acs.energyfuels.3c02587>.
- [67] A.R. Amani-Ghadim, M.S.S. Dorraji, Modeling of photocatalytic process on synthesized ZnO nanoparticles: Kinetic model development and artificial neural networks, *Appl. Catal. B: Environ.* 163 (2015) 539–546, <https://doi.org/10.1016/j.apcatb.2014.08.020>.
- [68] F. Yang, X. Yu, K. Wang, Z. Liu, Z. Gao, T. Zhang, J. Niu, J. Zhao, B. Yao, Photocatalytic degradation of methylene blue over BiVO₄/BiPO₄/rGO heterojunctions and their artificial neural network model, *J. Alloy. Compd.* 960 (2023) 170716–170725, <https://doi.org/10.1016/j.jallcom.2023.170716>.
- [69] F. Ghanbari, N. Modirshahla, M. Khosravi, M.A. Behnajady, Synthesis of TiO₂ nanoparticles in different thermal conditions and modeling its photocatalytic activity with artificial neural network, *J. Environ. Sci.* 24 (2012) 750–756, [https://doi.org/10.1016/S1001-0742\(11\)60815-2](https://doi.org/10.1016/S1001-0742(11)60815-2).
- [70] D.D. Upadhyay, A.K. Goyal, S. Maji, A. Dwivedi, G. Pandey, Biosynthesis of ZnO and TiO₂ nanoparticles using *Ipomoea carnea* leaf extract and its effect on black carrot (*Daucus carota* L.) cv. Pusa Asita, *Plant Physiol. Biochem.* 202 (2023) 107908–107918, <https://doi.org/10.1016/j.plaphy.2023.107908>.
- [71] D. Rede, L.H.M.L.M. Santos, S. Ramos, F. Oliva-Teles, C. Antão, S.R. Sousa, C. Delerue-Matos, Individual and mixture toxicity evaluation of three pharmaceuticals to the germination and growth of *Lactuca sativa* seeds, *Sci. Total Environ.* 673 (2019) 102–109, <https://doi.org/10.1016/j.scitotenv.2019.03.432>.



Sthefany Nunes Loureiro Academic in the chemical engineering course at Franciscan University.

Daniel Moro Druzian holds a degree in Materials Engineering from Universidade Franciscana (2018); a Master's degree in Nanosciences from Universidade Franciscana (2021) and is currently pursuing a PhD in Nanosciences from Universidade Franciscana (2021-2025). He has experience in Materials and Metallurgical Engineering, with an emphasis on Materials and Metallurgical Engineering, working mainly on the following topics: bone regeneration, biomaterials, nanotechnology, nanomaterials, agro-industrial waste and innovation, water treatment, adsorption, heterogeneous photocatalysis, material characterizations, in-silico tests, economic feasibility tests, development of technological products, correlations, clustering, in-vitro tests and ecotoxicity.

Leandro Rodrigues Oviedo Chemical Engineer from Franciscan University (2013-2018). Master in Nanosciences from Franciscan University (UFN). Worked as a Chemistry Teacher for the Alternative Popular Pre-University Extension Program (PUPA). Worked as a paid monitor in the disciplines of calculus I and II for engineering (2014-2015). Has the following extension courses: Unifra Languages - module I (2014); Basic Arduino (2015); Modeling and Simulation in Engineering Processes - Franciscan University (2016). Hygiene, health and beauty products (2017); Readings in English (2017). English Language Course at Topway English School-Santa Maria (2018). Supervised Curricular Internship in Quality, Safety, Environment and Health carried out at Thor Máquinas e Montagens LTDA (2018). Currently pursuing a PhD in the Postgraduate Program in Nanosciences. Research Line: reuse of waste for the synthesis of nanostructured materials.

Cristiane dos Santos holds a degree in Bioprocess Engineering and Biotechnology from the State University of Rio Grande do Sul (2010). Postgraduate MBA in Expertise, Auditing and Environmental Management (2012), Master in Materials Science - PGCIMAT-UFRGS (2014) and PhD in Materials Science - PGCIMAT - UFRGS (2021). She has experience in Product Research and Development, Sustainable Processes and Sol-Gel Processes to obtain hybrid and composite nanomaterials. CNPq Industrial Technological Development Scholarship - DTI-A - Franciscan University - UFN-RS (2023-2024).

Yolice Patricia Moreno Ruiz holds a bachelor's degree in Chemical Engineering (2006) and a master's degree in Chemical Engineering (2009) from the Universidad Nacional de Colombia (Medellín, Colombia) and a PhD in Chemical Engineering (2016) from the Universidade Federal do Rio Grande do Sul - UFRGS (Porto Alegre, Brazil). She has coordinated research projects in collaboration with the Federal University of Pernambuco - UFPE, the Center for Strategic Technologies of the Northeast - CETENE, the Aggeu Magalhães Institute of the Oswaldo Cruz Foundation - iLIKA (FIOCRUZ

Pernambuco), the Franciscan University - UFN (RS, Brazil), UFRGS (RS, Brazil) and the Polytechnic School of the University of São Paulo - USP (SP, Brazil). She has experience in engineering with emphasis on energy efficiency, heterogeneous catalysis, nanotechnology, supported metallocenes, ethylene polymerization, photocatalysis, small-angle X-ray scattering (SAXS) and sol-gel. Has theoretical and practical knowledge in structural and chemical characterization techniques of biomaterials, polymeric materials, nanostructures and nanocomposites. Develops research in materials chemistry, working on synthesis and characterization of nanostructures applied to agriculture, catalysis and health (multi-resistant bacteria). Works in the training of human resources in the undergraduate (PIBIC) and graduate programs at UFPE.

Giovani Pavoski Postdoctoral fellow in the Department of Materials Engineering at the University of British Columbia, Vancouver (UBC, 2023-2024). Postgraduate professor in the Department of Chemical Engineering of the Polytechnic School of the University of São Paulo in the subjects: Analytical Techniques in Environmental Chemical Engineering I and Analytical Techniques in Environmental Chemical Engineering II (2022-present). Bachelor's degree in Industrial Chemistry from the Pontifical Catholic University of Rio Grande do Sul (PUCRS-2012), master's degree (2014) and doctorate (2019) in Materials Science from the Federal University of Rio Grande do Sul (UFRGS-2019). Sandwich doctorate at the Autonomous University of Barcelona (UAB-Spain) in the Sandwich Doctorate Program Abroad (PDSE - CAPES). Experience with synthesis, characterization and processing of nanoparticles and polymeric nanocomposites. Dissertation and Thesis in the area of polymeric nanocomposites (polyethylene), with emphasis on the acquisition of electrical conductivity (graphene nanosheets) and antibacterial properties (silver nanoparticles covalently bonded or encapsulated in silica). Experience with synthesis, processing and characterization of polymers. Microbiology evaluating the antibacterial properties of nanocomposites. Research in the area of environmental chemistry with recycling and analysis of metals. Recycling of industrial catalysts through pyro/hydrometallurgical processes. Synthesis of metallic nanoparticles using secondary sources (catalyst waste, electronics, polymer composites) as raw material, aiming at a circular economy. Synthesis of magnetic nanoparticles for selective separation of critical metals. Currently a post-doctoral researcher participating in the FAPESP project, application of functionalized magnetic nanoparticles for the selective separation of lanthanum from solution resulting from the leaching of spent catalysts, at the Laboratory of Recycling, Waste Treatment and Extraction (LAREX), Department of Chemical Engineering of the Polytechnic School (POLI-USP) and University of British Columbia (UBC).

Jorge Alberto Soares Tenório Full Professor in the Department of Chemical Engineering of the Polytechnic School of the University of São Paulo. Metallurgical Engineer (1984), Master (1988) and Doctor (1992), Professor (1996) and Full Professor (2005) by the Department of Metallurgical and Materials Engineering of the Polytechnic School of the University of São Paulo. Sabbatical in the Department of Materials Science and Engineering of the Massachusetts Institute of Technology (2001). Works in the areas of Recycling, Solid Waste Treatment and Extractive Metallurgy. President of the ICTR-Institute of Science and Technology in Waste and Sustainable Development (2008-2011). Professor and guest advisor of the Materials Science and Engineering program of REDEMAT UFOP (2000-2015). Professor and guest advisor of the Master's Program in Metallurgical Engineering of the Federal Institute of Espírito Santo PROPEM IFES (2009-

2012). Editor of the Brazilian Journal of Environmental Sciences of the ICTR (2007-2014) and of the Metallurgy and Materials Section of the Escola de Minas Journal. Member of the CNPq Advisory Committee for Mining Engineering and Metallurgy and Materials (CA-MM) (2010-2013). Member of the Evaluation Committee of the Engineering II Area of CAPES (2004-2009). Coordinator of the Undergraduate Program (1989-1998), Coordinator of the Graduate Program (2002-2004), Head of Department (2010-2014) and Research Coordinator (2013-2014) of the Department of Metallurgical and Materials Engineering of the Polytechnic School. Member of the board of directors of CETESB (2019-). Coordinator of the EMBRAPII Tecnogreen Unit (2017-).

Denise Crocce Romano Espinosa Espinosa holds a degree in Metallurgical Engineering from the University of São Paulo (1995), and a master's and PhD in Metallurgical Engineering from the University of São Paulo, in 1998 and 2002, respectively. She did an 8-month research internship at the Massachusetts Institute of Technology (USA) in 2001 and was a visiting professor at the University of British Columbia (Canada) for a period of 12 months (2015-2016). From 2009 to 2014, she was an Associate Professor in the Department of Metallurgical and Materials Engineering of the Polytechnic School of USP. She was coordinator of the Postgraduate Program in Metallurgical Engineering of the Polytechnic School of USP (2012-2014), and alternate coordinator of the Research Committee of the Department of Metallurgical and Materials Engineering of EPUSP (2009-2012). She is currently an Associate Professor in the Department of Chemical Engineering at EPUSP, a full member of the Coordinating Committee of the Graduate Program in Chemical Engineering at EPUSP (2014-present) and Vice-Head of the Department of Chemical Engineering at EPUSP (2018-2022). She works as a Technical Advisor to the Office of the Superintendence of Environmental Management at USP (2018-2023) and is a representative of USP to the State Environmental Council (2020-2023). Her main areas of expertise are: recycling, waste treatment, hydrometallurgy, extractive metallurgy, and recycling of electro-electronic equipment.



William Leonardo da Silva Da Silva holds a degree in Chemical Engineering from the Federal University of Santa Maria (2010), a master's degree (2012) and a PhD (2016) in Chemical Engineering from the Federal University of Rio Grande do Sul. He developed research as a sandwich doctoral student abroad (PDSE/CAPES - 2015) at Ulster University with NIBEC (Nanotechnology and Integrated Bioengineering Centre). He is currently an adjunct professor II at the Franciscan University and a permanent professor of the Postgraduate Program in Nanosciences, coordinating the research group in applied nanomaterials (GPNAp). He has experience in the area of Green Nanotechnology, with emphasis on green synthesis of metallic nanoparticles, chemical kinetics and catalysis, working mainly on the following topics: removal of organic pollutants in wastewater by Advanced Oxidative Processes (heterogeneous photocatalysis) and by adsorption process, metallic nanoparticles and nanocatalysts.